White paper

Quantum HD with the NAEOTOM Alpha class

Clinical advantages of ultra-high resolution imaging using photon-counting CT

siemens-healthineers.com/naeotom-alpha

Thomas O'Donnell, PhD
Kristina Hallam, PhD
Elisabeth Shanblatt, PhD
Evrim Senol, MSc
Philipp Wolber, MSc
Matthew Fuld, PhD

SIEMENS Healthineers

Contents


SIEMENS
Healthineers
NAEOTOM Alpha

Introduction

Background

Ultra-High Resolution (UHR) imaging is crucial in radiology because it allows for the precise visualization of anatomical structures. The fine details captured in imaging can significantly impact diagnostic accuracy and treatment planning.

Spatial resolution, as defined by Radiopedia, refers to the ability of an imaging modality to differentiate two adjacent structures as distinct from one another. It is expressed in line pairs per cm (lp/cm). Improved spatial resolution enhances the definition and visibility of detail, enabling radiologists to make more confident diagnoses.

In this whitepaper, we explore the direct bearing of Quantum HD spatial resolution on clinical decision making with specific examples in thoracic, body, neurological, muscoloskeletal, pediatric, and cardiovascular imaging.

The technology

The trend in CT detector technology is moving towards smaller pixels to achieve better spatial resolution. Smaller pixels provide clearer visualization of small structures and textures, which could imply more diagnostic confidence. However, conventional Energy Integrating Detector CTs (EID-CTs) face challenges with radiation dose efficiency as pixel sizes decrease. Smaller pixels in EID-CTs suffer from geometric inefficiency, leading to reduced dose efficiency.

More specifically, these conventional EID-CT detectors employ a two-step process: first, the X-ray photon interacts with a scintillator to create visible light, which is then converted by a photodiode into an electric pulse to form the image. The primary challenge arises in the scintillator, where the created light can spread in any direction, including into neighboring detector elements.

Opaque barriers between detector elements, called septa, are required to prevent this optical crosstalk, but these septa also act as photon sinks, wasting any photon that lands on them. As the detector element size decreases, the space dedicated to septa increases, exacerbating the inefficiency. Alternatively, a comb may be placed between the patient and the detector to create the effect of smaller detector elements, thus blocking photons which have already passed through the patient. Again, resulting in a dose penalty.

Quantum HD is the UHR mode in NAEOTOM Alpha class photon-counting CT (PCCT) systems. It overcomes these challenges by removing the scintillation step in favor of a direct conversion of photons into an electric signal and thus eliminating the need for septa. The consequence is smaller pixels which allow for greater detail by avoiding the averaging of features under a larger pixel area. More detail means the system can tolerate more noise, allowing for lower doses while maintaining contrast-to-noise ratio (CNR) as expressed in a better Modulation Transfer Function (MTF) see Table 1.
The Vectron X-ray tube, capable of small focal spot of 0.4 × 0.5 mm at high power, is also key to achieving these gains in image quality.

High-contrast resolution with Quantum HD	
x-y plane	
50% MTF	39.0 lp/cm
10% MTF	42.9 lp/cm
2% MTF	44.3 lp/cm
Technique	120 × 0.2, 120 kV, 0.2-mm slices, Br98

Table 1: Modulation transfer function values of Quantum HD mode

"We have never been so excited to not understand what we are seeing."

Prof. Anders Persson,
Linkoping University Linkoping, Sweden

Specifics

The pixel dimensions of NAEOTOM Alpha in Quantum HD mode are 0.151 mm × 0.176 mm at the iso-center, capable of achieving a resolution of 0.11 mm in-plane. The resolution is 44.3 lp/cm at 2% of the MTF. The Quantum HD option is available for many of the protocols on NAEOTOM Alpha class systems and is indicated by a scan mode that includes "HighResUltra" in the name.

There are some limitations in invoking Quantum HD. These are not constraints due to physical phenomena but rather restrictions of implementation (i.e., the massive data transmission and processing capacities which are required). Collimation is currently limited to 120 detector rows of 0.2 mm slice thickness, and a non-spectral "T3D" reconstruction is required for slice thickness of 0.2 mm. While a high pitch of 3.2 is available for standard resolution scans, the lower bound on pitch is 0.2 and may vary depending on protocol. Spectral information may be available in Quantum HD mode but is limited to 0.4 mm standard resolution. Additionally, due to the requirement for a small focal spot, there are upper bounds on tube power.

Thorax imaging

Numerous scientific studies have reported on the clinical impact of Quantum HD in the thorax. For example, in a retrospective study, 112 consecutive patients with stable Interstitial Lung Disease (ILD) received both a standard resolution EID-CT scan and a Quantum HD PCCT scan within a median interval time of 12.8 months [1]. The classification of 4 of these patients changed from nonfibrotic (on standard resolution EID-CT) to fibrotic (on PCCT using Quantum HD) based "on differences in the depiction of focal areas of traction bronchiolectasis between [standard resolution EID-CT] (missed as blurred) and **Quantum HD** (sharp delineation)". Note that care was taken to ensure no differences were present due to an interim development of abnormalities. As an additional benefit, there was a mean dose reduction of 27% in the CTDI for the PCCT scan.

Another study reported an increased confidence in diagnosis of ILD using PCCT's Quantum HD compared to standard resolution EID-CT as evidenced by a reduction in the number of intermediate determinations made [2]. Specifically, "Photon-counting detector CT demonstrated a decreased number of indeterminate ground-glass opacities (GGO) (17 vs 26), an increased number of unlikely GGO (74 vs 50), and an increased number of likely reticulations (140 vs 130) relative to EID-CT."

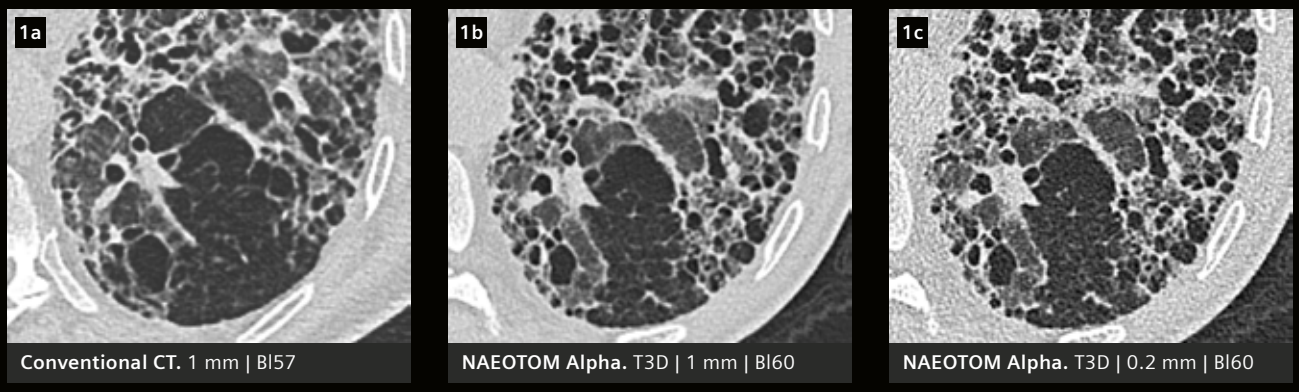

Figure 1: Comparison of standard resolution using 1 mm slice thickness on conventional CT (Fig. 1a), same slice thickness on NAEOTOM Alpha (Fig. 1b) and Quantum HD (Fig. 1c).
Courtesy of Erasmus Medical Center Rotterdam, Rotterdam, Netherlands.

Similarly, findings missed by resolution typical of conventional EID-CT, were discovered in a prospective study of COVID-19 patients using Quantum HD [3]. Patients were scanned using both types of CT on the same day and half of the patients showed some type of additional lung abnormality on Quantum HD. In particular, "non-specific GGO on EID CT images revealed to include fine reticulations, a possible sign of incipient pulmonary fibrosis, on **Quantum HD** scans in 6/20 (30%) participants."

Figure 1 and Figure 2 show examples of Quantum HD applied to the lung.

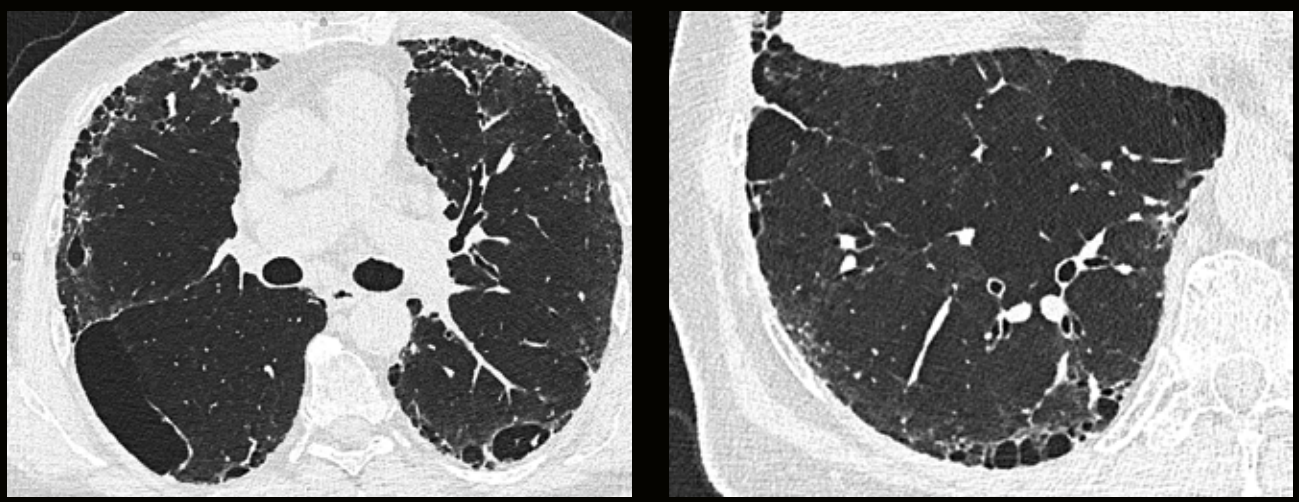

Figure 2: Extensive interstitial lung disease. T3D | 0.2 mm | Bl64 | Sn 140 kV | $CTDI_{vol}$: 2.27 mGy.
Courtesy of Erasmus Medical Center Rotterdam, Rotterdam, Netherlands.

Case study

Severe emphysema treated with endobronchial valves

Prof. Martine Rémy-Jardin, MD[1], Ph.D.; Prof. Jacques Rémy, MD[2]
[1] Department of Thoracic Imaging, University Centre of Lille, France
[2] Department of Radiology, Hospital Center of Valenciennes, France

History

A 53-year-old male with a significant smoking history (45 pack-years) and diagnosed with severe chronic obstructive pulmonary disease (COPD), specifically emphysema, was experiencing worsening dyspnea. The emphysema predominantly affected the right upper lobe (RUL). The patient underwent endobronchial valve (EBV) treatment aimed at reducing lung volume to improve respiratory function (see Figure 3).

Diagnosis

Pre-procedural Quantum HD chest CT confirmed the integrity of the right lung fissures, crucial for ensuring no collateral ventilation. Post-procedural Quantum HD, performed three months after EBV placement, showed successful valve positioning, complete atelectasis of the RUL, and improved diaphragm motion. The patient showed significant symptomatic improvement, including reduced dyspnea and better performance on the six-minute walk test.

Comments

COPD, specifically emphysema, is a progressive disease with no cure, but treatments like EBV can manage symptoms effectively. EBV treatment requires precise imaging to assess emphysema distribution and ensure no collateral ventilation, both of which are critical for treatment success. The Quantum HD acquisitions enable detailed anatomical visualization, essential for both pre- and post-procedural evaluations in EBV treatments, supporting optimal patient outcomes with lower radiation exposure.

Examination protocol	
Scan area	Thorax
Scan mode	UHR + Sn
Scan length	355 mm
Scan direction	Cranio-caudal
Scan time	3.7 s
Tube voltage	Sn 140 kV
Effective mAs	55 mAs
Dose modulation	CARE Dose4D
$CTDI_{vol}$	1.98 mGy
DLP	73.1 mGy*cm
Rotation time	0.25 s
Pitch	1.0
Slice collimation	120 × 0.2 mm
Slice width	0.2 mm
Reconstruction increment	0.2 mm
Reconstruction kernel	BI60, QIR4

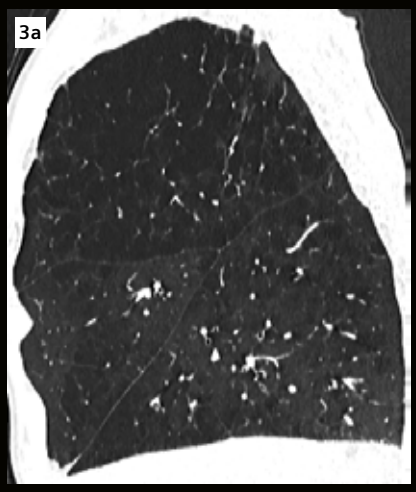

Figure 3a–b: A sagittal MPR image of the pre-EBV deposition (Fig. 3a) shows the completeness of the right major and minor fissures.
The same view of the post-EBV deposition (Fig. 3b) shows the upward and anterior displacement of the right major fissure with complete atelectasis of the RUL (arrowheads).
Courtesy of Department of Thoracic Imaging, University Centre of Lille, France.

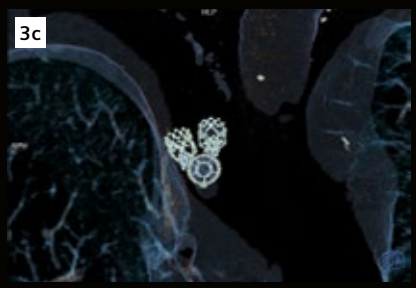

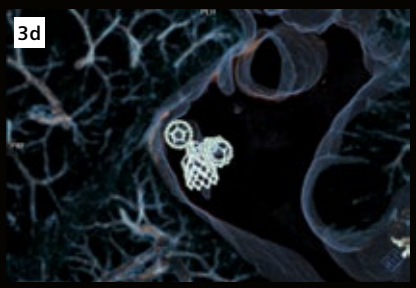

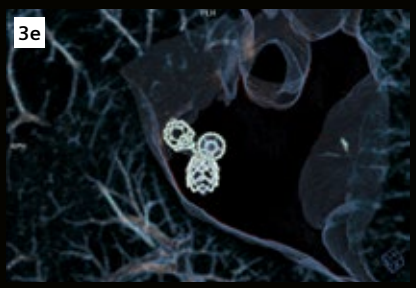

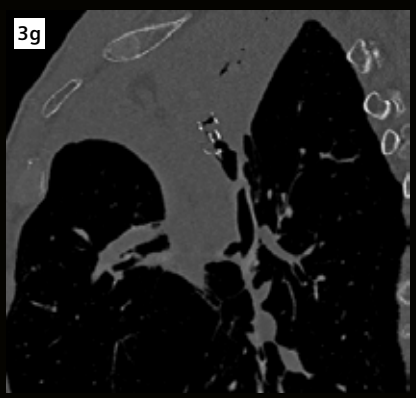

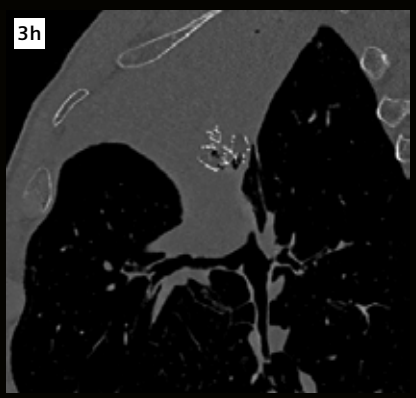

Figure 3c–h: cVRT images (Figs. 3c–e) and oblique MPR images (Figs. 3f–h) show three valves deposited in the right apical, posterior and anterior segmental bronchi and a completely collapsed RUL. Both cVRT and MPR views are reconstructed using 0.2 mm low-dose UHR images.
Courtesy of Department of Thoracic Imaging, University Centre of Lille, France.

Body imaging

Quantum HD has a role in body imaging as well. It has been observed that "Ultra-high-resolution imaging (UHR) is especially useful in the evaluation of lymph nodes," and further, "could prove to be useful in the categorization of pancreatic cancer." [4]

Figure 4 demonstrates the ability of Quantum HD to visualize the fine vascular anatomy of the abdomen. This technology may be useful for indications such as insulinoma/pre-catheter exam, stenosis of the mesenteric artery (abdominal pain), and pre-and post-transplantation or surgery.

The planning for oncological interventional procedures like TACE or SIRT requires a very detailed visualization and understanding of the vasculature supplying the tissue that should be addressed with the procedure. Missing small vessels that are feeding the tumor or – equally important – those that could be affected by the embolization but are supplying vitual tissue can negatively impact the outcome of the procedure. Clinical evidence of impact of UHR CT with photon-counting CT in such applications is still missing, but a positive effect should be expected.

1.0 mm | 0.4 mm | 0.2 mm | 1024² matrix each

Cinematic VRT based on 0.2 mm | 1024² matrix

Figure 4: Abdominal CTA. $CTDI_{vol}$: 6.3 mGy. Quantum Iterative Reconstruction Strength: 3. *Courtesy of Erasmus Medical Center Rotterdam, Rotterdam, Netherlands.*

In another study, an assessment of pancreatic adenocarcinoma with suspected lymph node and hepatic lesion involvement was performed. Progression was confirmed but surgery was deemed unnecessary (Figure 5).

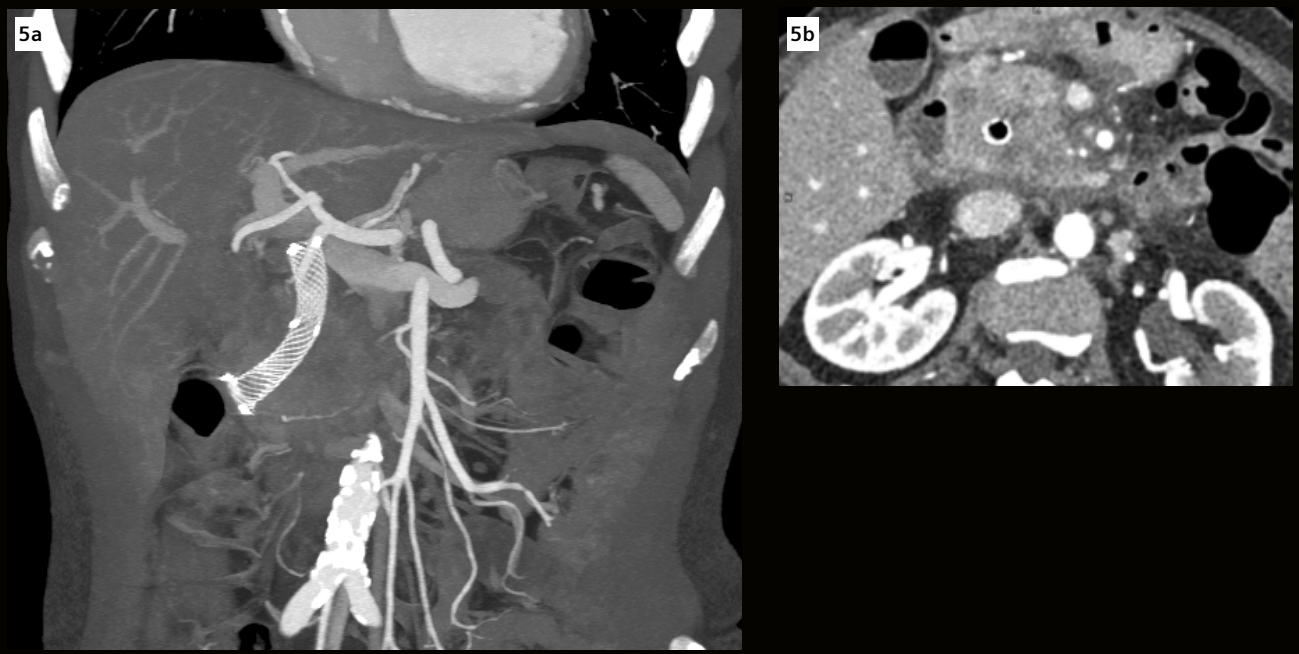

Figure 5: Coronal MIP (5a) | 0.2 mm MPR (5b) | Br36 | 140 kV | $CTDI_{vol}$: 5.52 mGy.
Courtesy of Gustave Roussy Institute, Villejuif, France

Case study

Pancreatic insulinoma in a patient with a history of hypoglycemia

Antonella Del Gaudio, MD; Daniele Marin, MD
Department of Radiology, Duke University, Durham, NC, USA

History

A 63-year-old female patient (BMI 19.57 kg/m²), with a history of hypothyroidism, fatigue, weakness, loss of appetite, and hypoglycemia, was referred to the Department of Radiology for evaluation. A calcium stimulation challenge test showed diffuse insulin secretion throughout the pancreas. A pancreatic insulinoma was suspected. However, a previous CT examination performed with an EID-CT did not reveal any pancreatic lesion. A contrast CT scan with a NAEOTOM Alpha was performed for further evaluation.

Diagnosis

Virtual monoenergetic images (VMIs), displayed at 50 KeV, revealed a hypervascular nodular lesion in the pancreatic body in the arterial phase, measuring 1 cm in size. The lesion was also seen in the iodine maps and the VNC/iodine fused images. In the virtual non-contrast (VNC) images, it appeared isodense, and in the standard image reconstructions, it was inevident. Subsequently, the lesion was confirmed by a Dotatate PET/CT scan as well as an Endoscopy Ultrasound (EUS) examination. The patient underwent a distal pancreatectomy with splenectomy. The pathology result confirmed the diagnosis of a G1 well-differentiated neuroendocrine tumor with insulin hyperproduction.

Examination protocol	
Scan area	Abdomen / Abdomen-Pelvis
Scan mode	UHR / Quantumplus (Arterial / venous phases)
Scan length	249.6 / 423.2 mm
Scan direction	Cranio-caudal
Scan time	5.2 / 4.5 s
Tube voltage	140 kV
Effective mAs	156 / 67 mAs
IQ level	280 / 227
Dose modulation	CARE Dose4D
$CTDI_{vol}$	18.2 / 7.7 mGy
DLP	487 / 352 mGy*cm
Rotation time	0.5 s
Pitch	1.0 / 0.8
Slice collimation	120 × 0.2 / 144 × 0.4 mm
Slice width	0.2, 0.4 / 0.4 mm
Reconstruction increment	0.2 / 0.4 mm
Reconstruction kernel	Br48, Qr40 / Qr40
keV level	50 keV
Spectral reconstruction	Monoenergetic Plus
Contrast	**300 mg/mL**
Volume	150 mL
Flow rate	4 mL/s
Start delay	1, Arterial phase: bolus tracking triggered at 150 HU in the descending aorta + 17 s 2, Venous phase: 45 s

Comments

Insulinoma is a type of functional pancreatic neuroendocrine tumor (pNET) originating from the endocrine cells of the pancreas. It is often confined to the pancreatic gland and characterized by hypersecretion of insulin causing hypoglycemia. Surgery is the only potentially curative therapeutic strategy in localized disease, and generally, small pancreatic insulinomas have a very good prognosis [5]. The challenge, though, lies in the identification of the primary tumor due to its small size.

PCD-CT provides energy-resolved CT data with increased spatial resolution and inherent spectral information [6]. Tissue contrast is optimized by a combination of the lack of down-weighting of the lower energy X-ray photons and the removal of electronic noise. In this case, a UHR mode was performed, using a fine collimation of 120 x 0.2 mm, in the arterial phase. VMIs were then reconstructed at 0.4 mm and displayed at 50 keV to enhance the contrast. The small insulinoma, initially missed by EID-CT, is clearly visualized owing to the combination of increased spatial resolution and tissue contrast. This facilitates an appropriate surgical planning and thereby an optimal patient outcome.

Figure 6: An axial VMI, acquired in the arterial phase and displayed at 50 keV, shows a small hypervascular nodular lesion in the pancreatic body (Fig. 6c, arrow). The lesion is neither shown in a previous EID-CT image (Fig. 6a) nor evident in a standard image reconstruction (Fig. 6b).

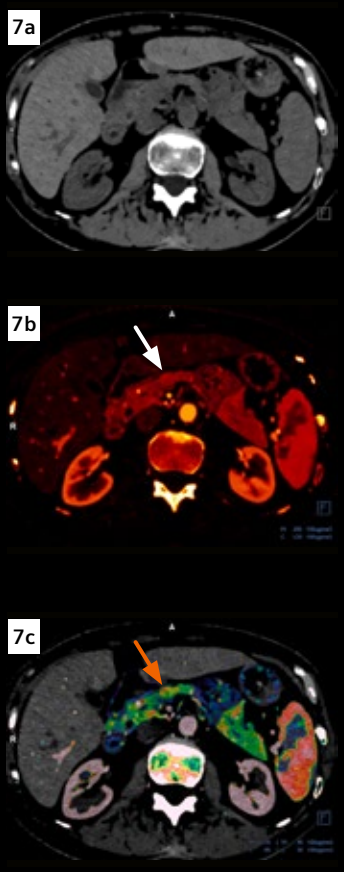

Figure 7: An iodine map (Fig. 7b) and a VNC/iodine fused image (Fig. 7c) show a contrast enhanced lesion (arrows) in the pancreatic body.The lesion appears isodense in the VNC image (Fig. 7a)

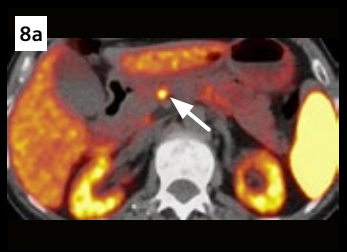

Figure 8: A Dotatate PET/CT image shows a small lesion spotted in the pancreatic body (Fig. 8a, arrow). The lesion is clearly seen in a cinematic VRT image created with Quantum HD images as well (Fig. 8b, arrow).
Courtesy of Department of Radiology, Duke University, Durham, NC, USA

Neurological imaging

Cochlear implants

Cochlear implants (CIs) bypass damaged or nonfunctional parts of the ear and directly stimulate the auditory nerve. UHR imaging is often used in the workup prior to and assessment after their deployment. The detailed information provided by UHR imaging helps assessing candidates, and in the planning of the procedure, supporting the accurate and effective placement of the implant. After the implant has been placed, it can help verify the position of the electrodes within the cochlea. This allows for the implant to be positioned correctly, functioning as intended, and may detect other complications (e.g., cochlear ossification) [7].

Quantum HD has the potential to not only reduce the dose of UHR imaging in cochlear implant assessment compared to EID-CT, but can also improve the overall image quality. In contrast with conventional EID-CT, Quantum HD reduced dose by an average of 22% while having significantly better visualization. "Compared to multi-detector CT, the visibility of the normal temporal bones scored better with PCCT" [8]. Indeed, Jeremy Wales, ENT specialist and Senior Researcher in Otology at Karolinska University Hospital, Sweden, says "NAEOTOM Alpha with Quantum HD imaging enables visualization of the exact CI electrode placement within the cochlea while also minimizing the radiation dose."

Figure 9 and Figure 10 provide examples of the high image quality Quantum HD brings to the visualization of cochlear implants.

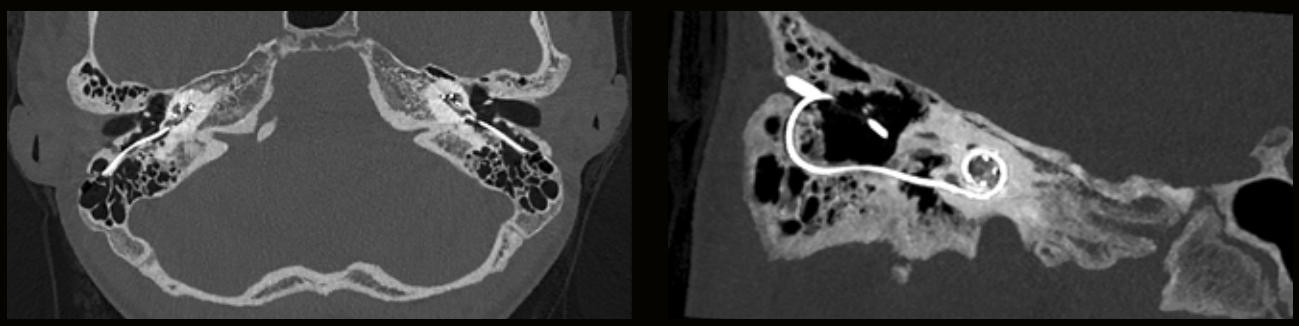

Figure 9: Bilateral implants, Quantum HD. 120 kVp | CTDI: 11 mGy | MPRs | 0.2 mm | Hr72.
Courtesy of University Hospital of Karolinska, Stockholm, Sweden.

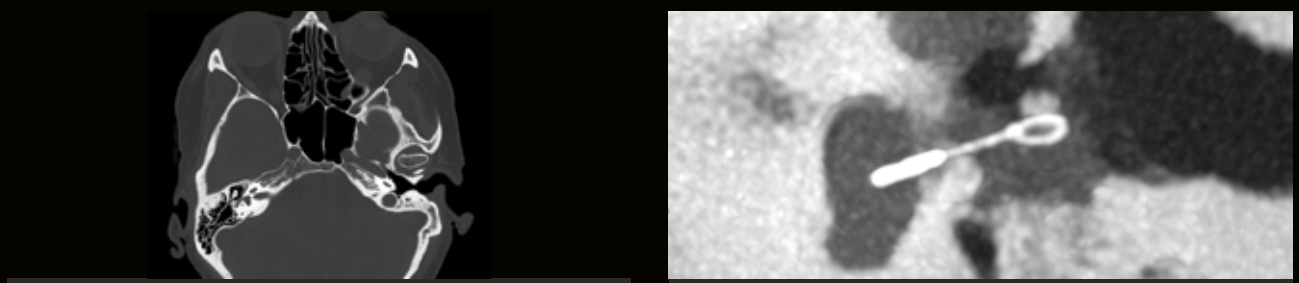

Figure 10: CT imaging of the skull base for stapes implant follow-up. Quantum HD | CTDI: 55 mGy | QIR strength: 3.
Courtesy of Erasmus Medical Center Rotterdam, Rotterdam, Netherlands.

Cerebrovascular exams

Quantum HD also has the potential to transform vascular imaging in the head. A comparison of angiographic images of the orbital vasculature between EID-CT (Dual Energy 100/Sn 150 kV) and PCCT's Quantum HD at comparable doses found the "arterial anatomy of the orbit is much better depicted with arterial Quantum HD as opposed to arterial EID-CT" [9]. Furthermore, "Angiographic Quantum HD of the orbit could potentially obviate conventional catheter-based examinations in certain clinical situations where the diagnosis or appropriate follow-up imaging can be made adequately with CTA. Angiographic Quantum HD should also be able to reliably assess for potential collaterals which could contraindicate or modify approach of certain therapeutic interventions.

In this domain, Quantum HD has demonstrated its utility in a variety of contexts. For example: Figure 11 shows an example of Quantum HD allowing the depiction of micro-calcifications in the ophthalmic and superficial temporal arteries.

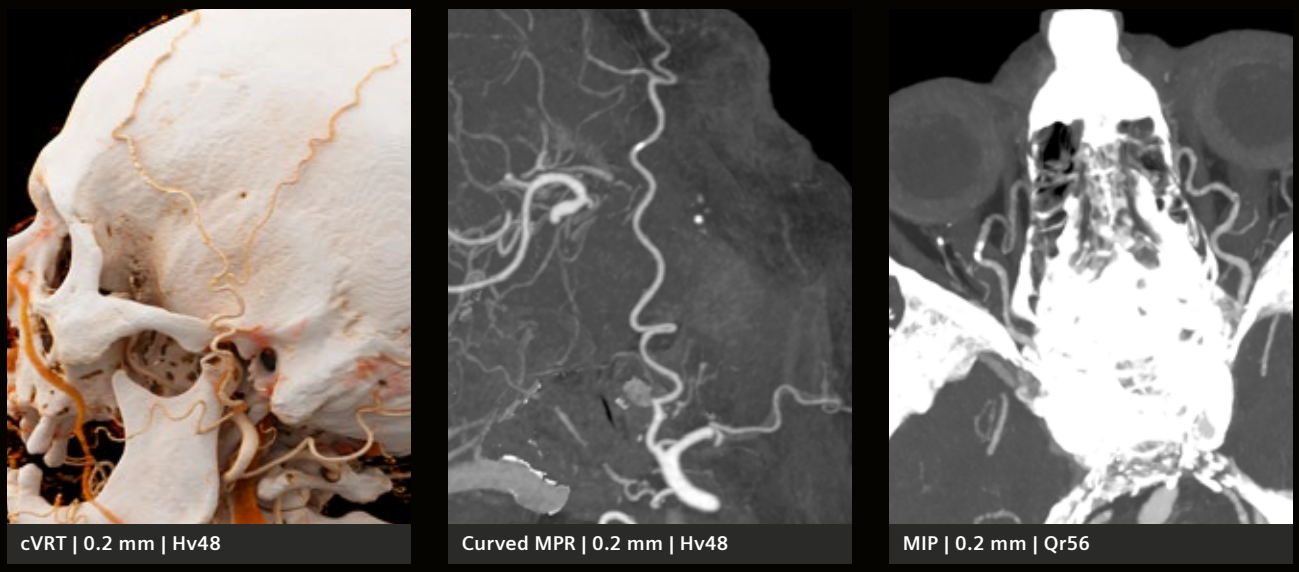

Figure 11: Ophthalmic and superficial temporal arteries. Quantum HD | 120 kVp | CTDI: 10 mGy.
Courtesy of Erasmus Medical Center Rotterdam, Rotterdam, Netherlands.

Figure 12 shows a carotid artery and a middle cerebral artery stent with dimensions 20 mm long by 2 mm wide. Note the lack of blooming artifact due in part to the high-resolution characteristics of Quantum HD. Figure 13 also lacks any major metal artifacts in Quantum HD mode and maintains the contrast in the small vessels. Figure 14 depicts an aneurysm less 3 mm in diameter.

Lacrimal duct imaging

Quantum HD is also capable of imaging beyond the vasculature to evaluate the patency of the lacrimal duct. Figure 15 depicts a case study of a patient whose lacrimal duct was not filling. The stakes in this case were high since the patient, after extensive facial reconstruction, had only one eye. If this eye were compromised the patient would be completely blind. A procedure was performed to inject contrast into the duct and follow its path. PURE Lumen was applied to the spectral reconstruction as well to virtually remove any microcalcifications.

Cerebrospinal fluid venous fistula

A CVF (Cerebrospinal fluid venous fistula) is an abnormal connection between the cerebrospinal fluid (CSF) space and the venous system, allowing CSF to leak directly into the veins. This can lead to a variety of symptoms and complications, often painful. Diagnosis and detection of CVF can be extremely challenging. The size of the fistula can be very small and sometimes require very dense intrathecal contrast for the draining vein to become visible. This contrast agent may also be rapidly washed away by the

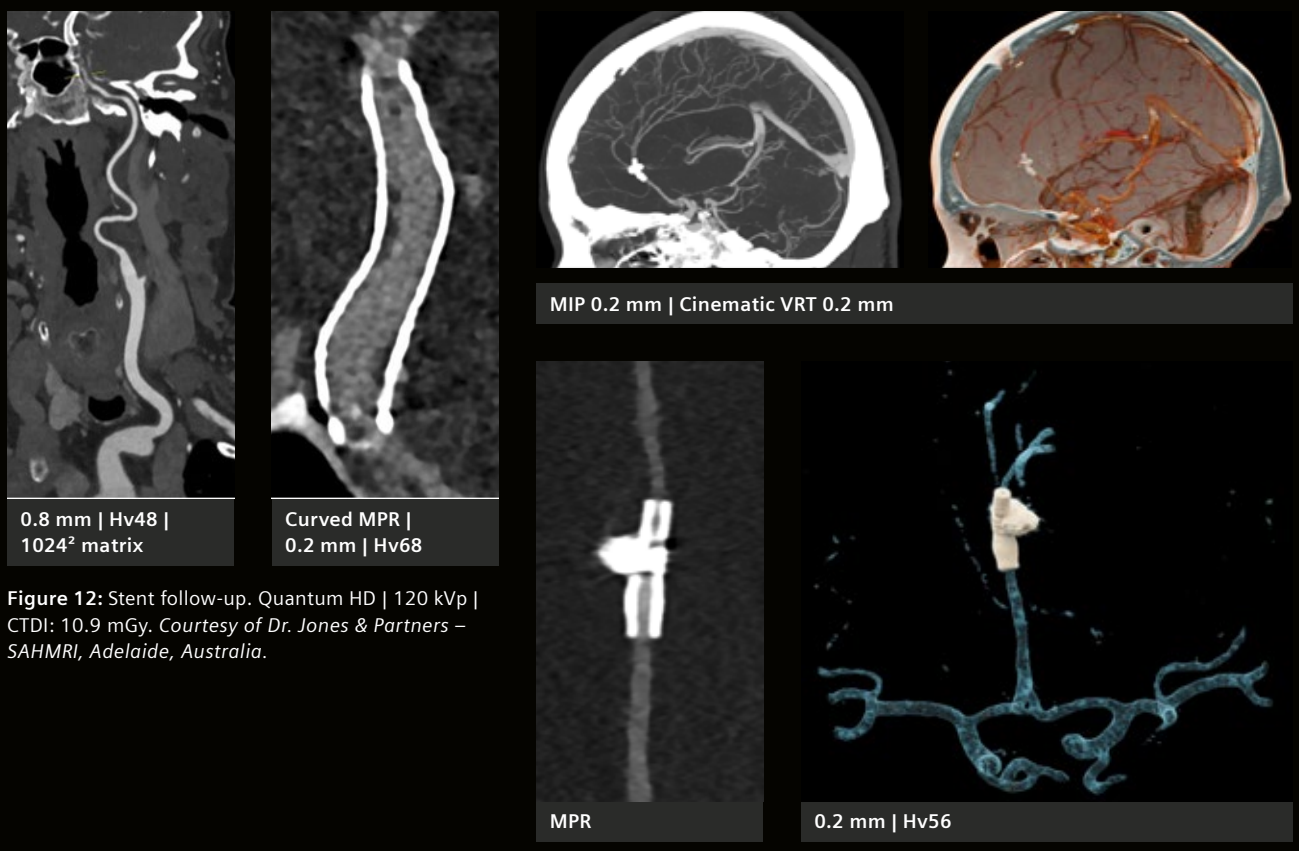

Figure 12: Stent follow-up. Quantum HD | 120 kVp | CTDI: 10.9 mGy. *Courtesy of Dr. Jones & Partners – SAHMRI, Adelaide, Australia.*

Figure 13: Flow Diverter. Quantum HD | 120 kVp | CTDI: 14 mGy. *Courtesy of Erasmus Medical Center Rotterdam, Rotterdam, Netherlands.*

venous system complicating the timing of detection. Additionally, the anatomical regions where CSF fistulas occur are complex and may be obscured by surrounding structures. And, the fistula's appearance or the symptoms thereof may be intermittent. Finally, the rate of leakage can vary or may only be apparent during certain activities or body positions. As a result, CVFs may often be missed or undetectable [10].

Recent studies have looked at PCCT's capabilities for the detection of CVFs versus other approaches. In a 38-patient intraindividual comparison between non-UHR EID-CT and Quantum HD PCCT myelography, it was shown that for the task of detecting CVFs, PCCT's Quantum HD yielded significantly higher sensitivity without a loss of specificity [11]. Overall image quality was better, and it was noted that "improved visualization of the spinal nerve root sleeves may assist radiologists in detecting subtle nerve root abnormalities and assessing the precise extent of CVF leakage, in turn possibly assisting patient management." The authors cite the greater spatial resolution of Quantum HD as a major factor in detecting small CVFs.

In another study, 8 patients who had both EID-CT and PCCT myelography were collected through a retrospective search of PACS [12]. In every case, the EID-CT had deemed the patient CVF-negative while PCCT's Quantum HD found a definitive CVF. Similarly, in comparing 39 patients who had both Digital Subtraction Myelography (DSM) and PCCT myelography, 33 of the patients identified as having a CVF on PCCT had a negative result for DSM.

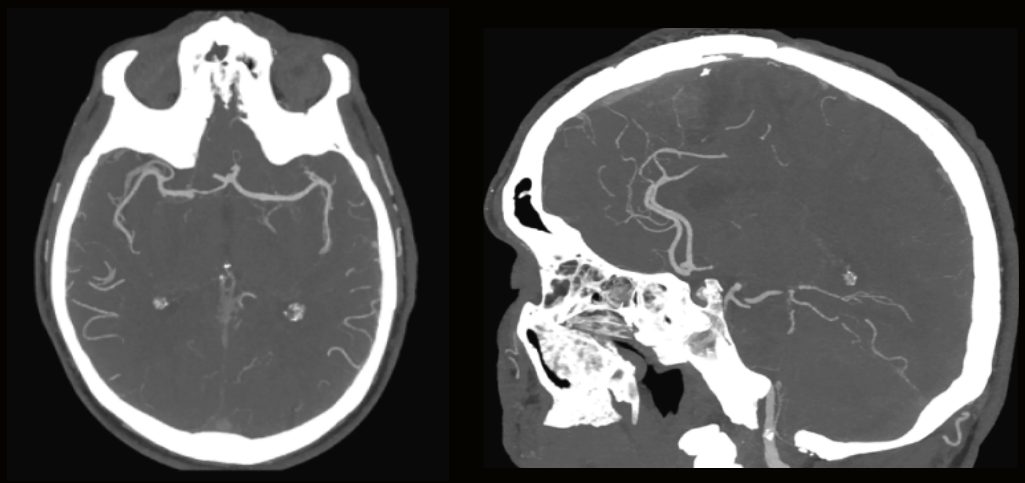

Figure 14: Aneurysm less than 3 mm in diameter. Quantum HD | 120 kVp | $CTDI_{vol}$: 14.5 mGy | DLP: 261 mGy*cm.
Courtesy of Erasmus Medical Center Rotterdam, Rotterdam, Netherlands.

As part of this study, overall, patients with low probability of having CVF based on MR evaluation of intracranial hypotension appeared to have a better yield of detection using Quantum HD compared to other modalities. The authors point out that the high spatial resolution of Quantum HD "is invaluable for detecting contrast within tiny veins, or even a thin column of contrast within a larger vein. High spatial resolution also helps to distinguish small internal epidural veins from the adjacent thecal sac or veins adjacent to diverticula."

While the focus of this whitepaper is UHR, we would be remiss to not point out other advantages that PCCT brings in addressing the challenge of detecting CVFs.

First, the fast acquisition time may reduce respiratory and patient movement artifacts (EID may also provide fast acquisition but at the expense of simultaneous UHR and spectral analysis). It also provides freedom for multiple time points to be scanned since it is not always clear whether early or delayed imaging is more appropriate for diagnosis in an individual [13]. Second, PCCT can provide spectral information in every exam, allowing low keV VMI reconstructions to be made which can boost iodine conspicuity [13]. Finally, in comparison to EID-CT, lower radiation exposure is possible [11].

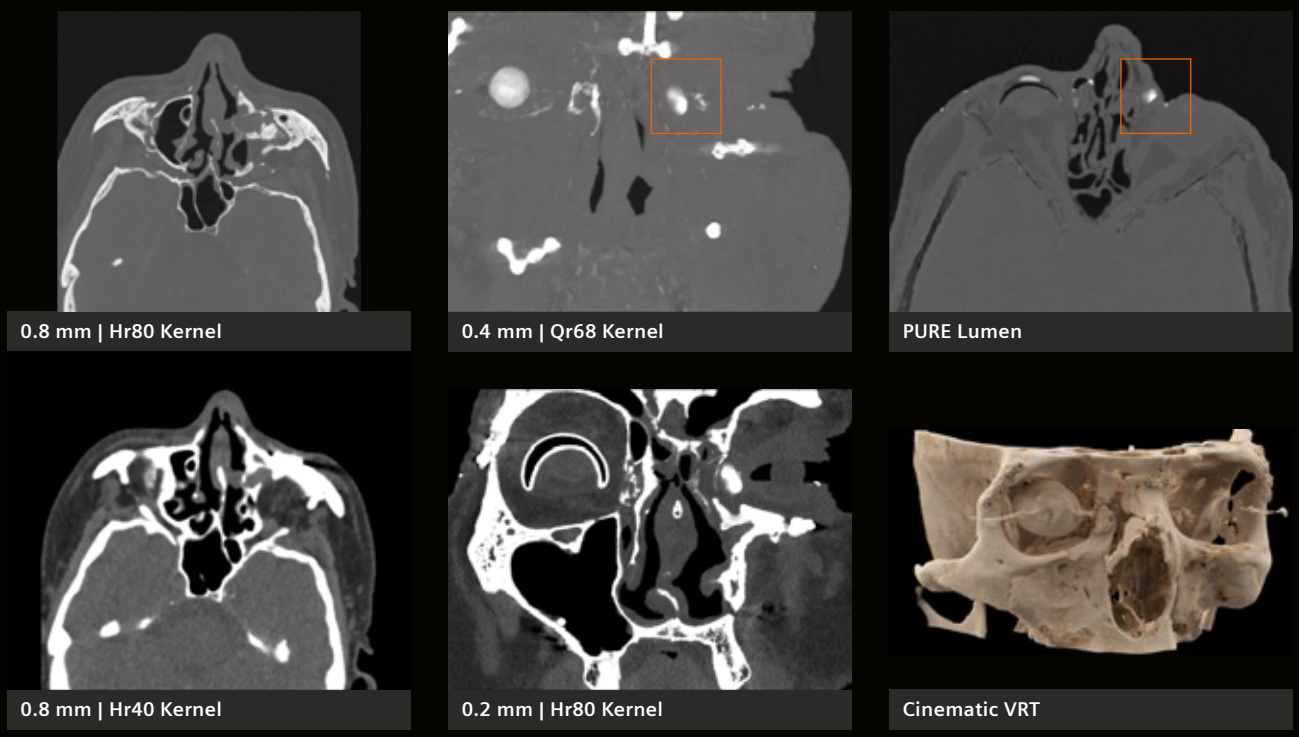

Figure 15: Contrast agent injected into patient's lacrimal duct to evaluate patency. Pre-contrast scan: CTDI 7.79 mGy; post-contrast scan: Quantum HD CTDI 21.4 mGy. *Courtesy of Erasmus Medical Center Rotterdam, Rotterdam, Netherlands.*


SIEMENS
Healthineers

Case study

Cerebrospinal fluid venous fistula

Fides Regina Schwartz, MD; Timothy Amrhein, MD
Department of Radiology, Duke University Health System, North Carolina, USA

History

A 58-year-old female with a 10-year history of migraine, tinnitus, and orthostatic headache was evaluated for suspected Spontaneous Intracranial Hypotension (SIH). A previous MRI confirmed SIH, but prior attempts to locate the spinal cerebrospinal fluid venous fistula (CVF) causing the issue were unsuccessful (see Figure 16).

Diagnosis

- Previous CT myelography (CTM) using EID-CT at 0.625 mm slice thickness failed to identify the CVF.
- CTM performed using Quantum HD at 0.2 mm slice thickness successfully identified the sub-millimeter CVF at the right T5 level.
- Iodine map and 3D images from cinematic volume rendering technique (cVRT) were used to confirm diagnosis.
- Dose reduction of 79% for PCCT compared to EID-CT (8.6 mGy with PCCT vs. 41.3 mGy with EID-CT).

Outcome

- The precise localization of the CVF allowed for surgical ligation, which was successful.
- The patient's symptoms resolved, and follow-up brain MRI showed normalization of SIH-related findings.

Examination protocol	
Scan area	Spine
Scan mode	UHR (Quantum HD)
Scan length	354 mm
Scan direction	Caudo-cranial
Patient position	FFDR (Feet First Decubitus Right)
Scan time	7.6 s
Tube voltage	140 kV
Effective mAs	74 mAs
Dose modulation	CARE Dose4D
$CTDI_{vol}$	8.58 mGy
DLP	341 mGy*cm
Rotation time	0.5 s
Pitch	0.85
Slice collimation	120 × 0.2 mm
Slice width	0.2 mm
Reconstruction increment	0.2 mm
Reconstruction kernel	Br48u, QIR 4
Contrast	Iopamidol (300 mg/mL)
Volume	10 mL
Flow rate	Manual injection

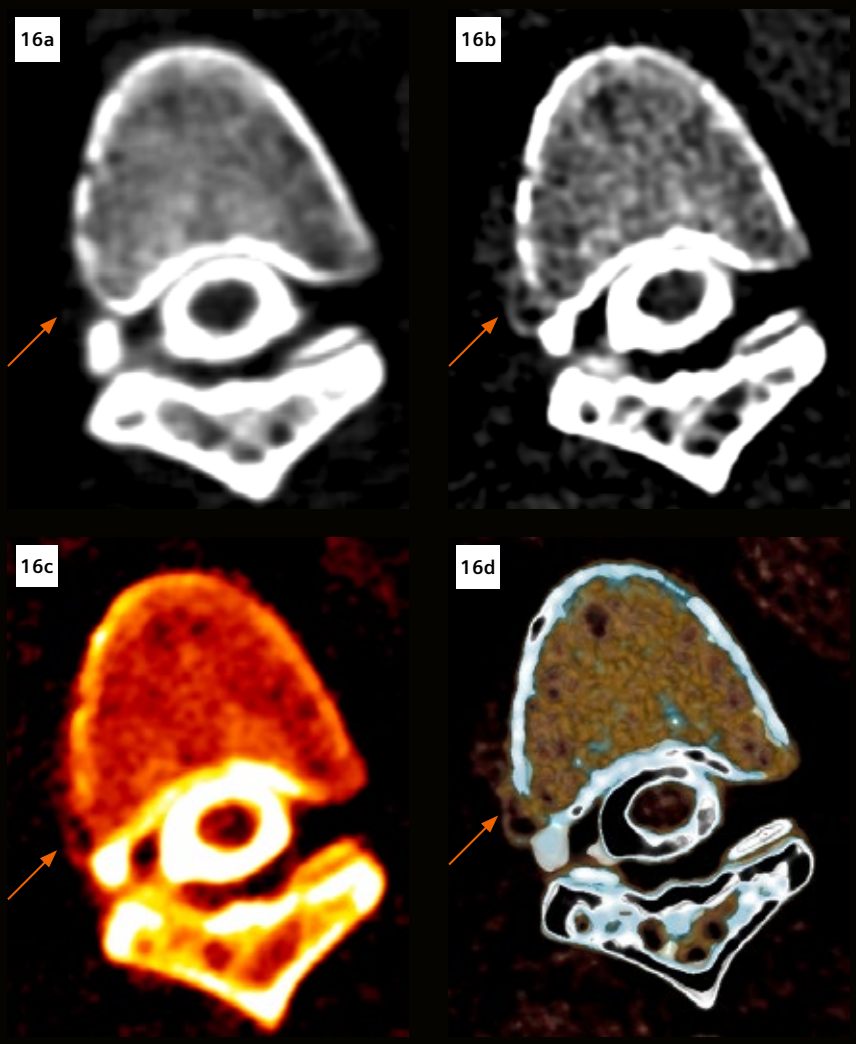

Figure 16: Detection of CVF. Quantum HD | Br48 | QIR 4 | Feet First Decubitus Right | 140 kV | CTDI: 8.58 mGy.
Fig 16a: An axial image, acquired at 0.625 mm on an EID-CT at the level of T5 shows a prominent nerve root sleeve visible to the right of the spinal canal (arrow). A CVF is not apparent.

Fig. 16b: A UHR image, acquired at 0.2 mm on PCCT shows a prominent nerve root sleeve (arrow) and a visible CVF at the same level (arrow).

Fig. 16c: An iodine map (0.4 mm).

Fig. 16d: A thin slab cVRT image shows the CVF (arrows) at the same location.
Courtesy of Department of Radiology Duke University Health System, Durham, NC, USA.

Musculoskeletal imaging

Several studies have documented the improved appearance of bone structures when applying Quantum HD on NAEOTOM Alpha as compared to comb-induced UHR on EID-CT. For example, cadaver experiments showed that "PCD-CT allows for a twofold higher visibility of bone structure sharpness and an overall improved image quality of the wrist compared to images obtained from an UHR EID-CT. Even at half dose, Quantum HD yielded superior image quality, both in quantitative measures and as evaluated by radiologists" [14]. This improved sharpness extends to the evaluation of elbow fractures as shown in a different cadaver study [15]. According to the authors, "Quantum HD provided superior objective and subjective image quality for fracture and trabecular bone structure delineation of the elbow compared to UHR EID-CT in a typical post-trauma setting." This view was reinforced in a patient study touting Quantum HD's superior fracture visibility and overall image quality [16]. Indeed, the quality of Quantum HD has even been compared to microCT [17].

Figure 17 illustrates the application of Quantum HD in a pediatric case of osteochondritis dissecans of the capitellum.

Figure 17: MPR 0.2 mm (Fig 17a) | Cinematic VRT (Fig 17b–d) | Br89 | 120 kV | $CTDI_{vol}$ 4.5 mGy
Courtesy of Erasmus Medical Center Rotterdam, Rotterdam, The Netherlands

Combining UHR and functional imaging: Quantum HD and Bone Marrow Edema

The Bone Marrow Edema (BME) application is particularly valuable in situations where fractures are so subtle that they may be hard to detect on conventional CT. In these cases, it may be possible to indirectly diagnose trauma through the suggestion of edema [18]. However, the potential of combining the increased resolution of Quantum HD with the spectral analysis of BME shows significant promise. Figure 18 illustrates the clinical potential of combining Quantum HD with BME.

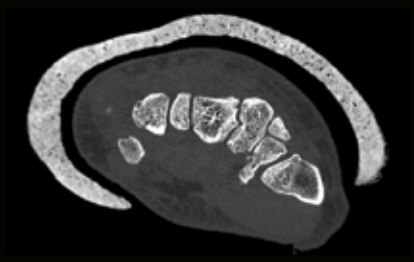

MPR | 0.2 mm | Br89

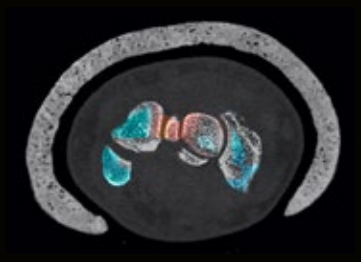

MPR Fused | 0.2 mm | Br89

MPR | 0.2 mm | Br89

MPR Fused | 0.2 mm | Br89

Figure 18: Quantum HD fused with Bone Marrow Edema visualization. Sn 150 kV / 70 kV | CTDI 4.7 mGy.
Courtesy of University Hospital Minden, Minden, Germany.

Case study

Osteochondritis dissecans of the capitellum

Ronald Booij, Ph.D.; Prof. Edwin Oei, MD, Ph.D.
Department of Radiology & Nuclear Medicine, Erasmus MC Rotterdam, Rotterdam, The Netherlands

History

A 13-year-old female patient, a gymnast, with left elbow complaints for the past 18 months, presented herself to the hospital. A radiograph of the elbow showed a suspicious osteochondritis dissecans (OCD) of the capitellum. To further evaluate the dimension of the lesion and the possible existence of loose fragments, a Quantum HD was requested.

Diagnosis

The UHR CT images showed a cortical defect at the capitellum of the left humerus, with an approximate size of 9.2 mm (coronal) x 9.8 mm (sagittal) x 4.1 mm (depth) on the medial side. There were two loose fragments – one was about 5.1 mm in size, next to the capitellum, and the other was about 6.2 mm in size, seen dorsally on the lateral side of the olecranon. There were no signs of any focal osseous abnormalities elsewhere, nor evidence of focal muscle abnormalities. The trabeculation of the radial head was normal.

CT findings suggested an OCD focus at the capitellum of the left humerus with two loose bone fragments, demonstrating an unstable lesion. Subsequently, the patient was scheduled for arthroscopic surgery.

Comments

OCD is a disorder of the articular cartilage and subchondral bone which most commonly occurs in adolescent athletes [19]. In the elbow, it typically affects the humeral capitellum. Early recognition and appropriate intervention may protect adolescents from fragmentation of the OCD lesion and the development of irreversible cartilage damage. It is important to differentiate between stable and unstable OCD lesions, hereby is a CT considered more sensitive than a radiograph, to determine the best treatment option [20]. An unstable lesion would require a surgical approach, and prior to that, it would be essential to acquire detailed diagnostic information, such as the lesion size, the stability and viability of the lesion fragment, and the number of present loose bodies, for surgical planning.

UHR images are acquired at 0.2 mm slice width and reconstructed using a very sharp kernel (Br89) with a 2% value of the modulation transfer function of 31 lp/cm. This provides improved visualization of the cortical and trabecular bone microarchitecture, enhancing the diagnostic confidence of the radiologists. Traditionally, with conventional CT, UHR images are associated with higher image noise and require higher radiation dose. However, PCCT enables UHR scanning without substantial increase in image noise, because UHR scan data are acquired at full dose efficiency without additional combs or grids to reduce the detector aperture, and image noise is further reduced by a refined model-based iterative reconstruction approach (Quantum Iterative Reconstruction, QIR). The low image noise even enables the use of the UHR images for cinematic volume rendering technique (cVRT), providing a photo-realistic 3D visualization and facilitating surgery planning. Potentially, image noise reduction also leads to a reduction of the radiation dose, which is important especially for young patients. As shown in this case, the combination of improved spatial resolution with reduced image noise, provided by Quantum HD imaging with PCCT, benefits musculoskeletal imaging.

Examination protocol	
Scan area	Left elbow
Scan mode	Quantum HD
Scan length	103 mm
Scan direction	Caudo-cranial
Scan time	3.8 s
Tube voltage	120 kV
Effective mAs	56 mAs
Dose modulation	CARE Dose4D

$CTDI_{vol}$	4.5 mGy
DLP	50.8 mGy*cm
Rotation time	0.5 s
Pitch	0.55
Slice collimation	120 x 0.2 mm
Slice width	0.2 mm
Reconstruction increment	0.1 mm
Reconstruction kernel	Br89, QIR3

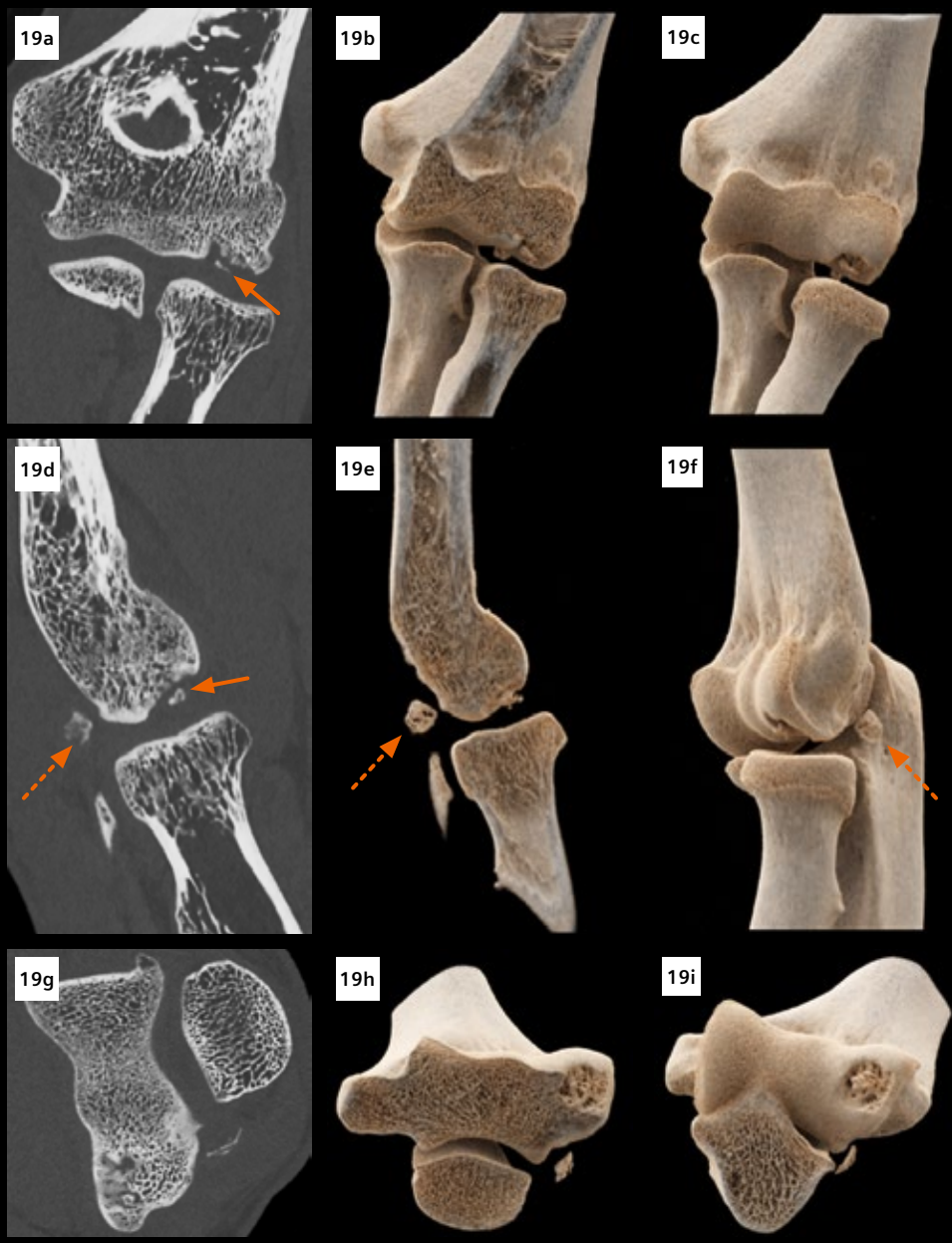

Figure 19: MPR images (Figs. 19a, 19d & 19g) and cVRT images (Figs. 19b, 19c, 19e, 19f, 19h & 19i), reconstructed in 3D views, show a cortical defect at the capitellum of the left humerus with two loose fragments – one next to the capitellum (arrows), and the other seen dorsally on the lateral side of the olecranon (dotted arrows). The trabeculation of the radial head shows normal structures. Note that the input images for cVRT creation are reconstructed with 0. 2mm slice thickness and a very sharp kernel of Br89.
Courtesy of Department of Radiology & Nuclear Medicine, Erasmus MC Rotterdam, Rotterdam, The Netherlands

Case study

Fall on outstretched hand (FOOSH)

Ronald Booij, Ph.D.; Prof. Edwin Oei, MD, Ph.D.
Department of Radiology & Nuclear Medicine, Erasmus MC Rotterdam, Rotterdam, The Netherlands

History

A 20-year-old male underwent screw fixation for a scaphoid fracture caused by a FOOSH. After experiencing non-union of the fracture, a revision surgery was performed four years later. Follow-up imaging using traditional CT was hindered by metal artifacts, prompting an acquisition using Quantum HD on NAEOTOM Alpha.

Diagnosis

The UHR CT images provided clear visualization of the scaphoid fracture, the fixation screw, and surrounding bone structures.

Key findings included:

- A visible scaphoid fracture with a sclerotically bordered fracture line and minimal central bridging.
- Screw loosening indicated by lucency around the screw and its protrusion into the radiocarpal joint.
- Early osteoarthritic changes and slight dorsal tilting of the lunate. These detailed images facilitated the decision to schedule the patient for surgical revision.

Conclusion

The use of Quantum HD in this case highlighted its significant clinical benefits, including high-resolution imaging, effective metal artifact reduction, low radiation dose, and 3D visualization. These advancements facilitated accurate diagnosis, informed surgical planning, and enhanced overall patient care.

Examination protocol	
Scan area	Wrist
Scan mode	UHR mode
Scan length	48.3 mm
Scan direction	Caudo-cranial
Scan time	3.5 s
Tube voltage	Sn 140 kV
Effective mAs	216 mAs
Dose modulation	CARE Dose4D
$CTDI_{vol}$	7.8 mGy
DLP	65.3 mGy*cm
Rotation time	0.5 s
Pitch	0.4
Slice collimation	120 × 0.2 mm
Slice width	0.2 mm
Reconstruction increment	0.1 mm
Reconstruction kernel	Br89, QIR 3

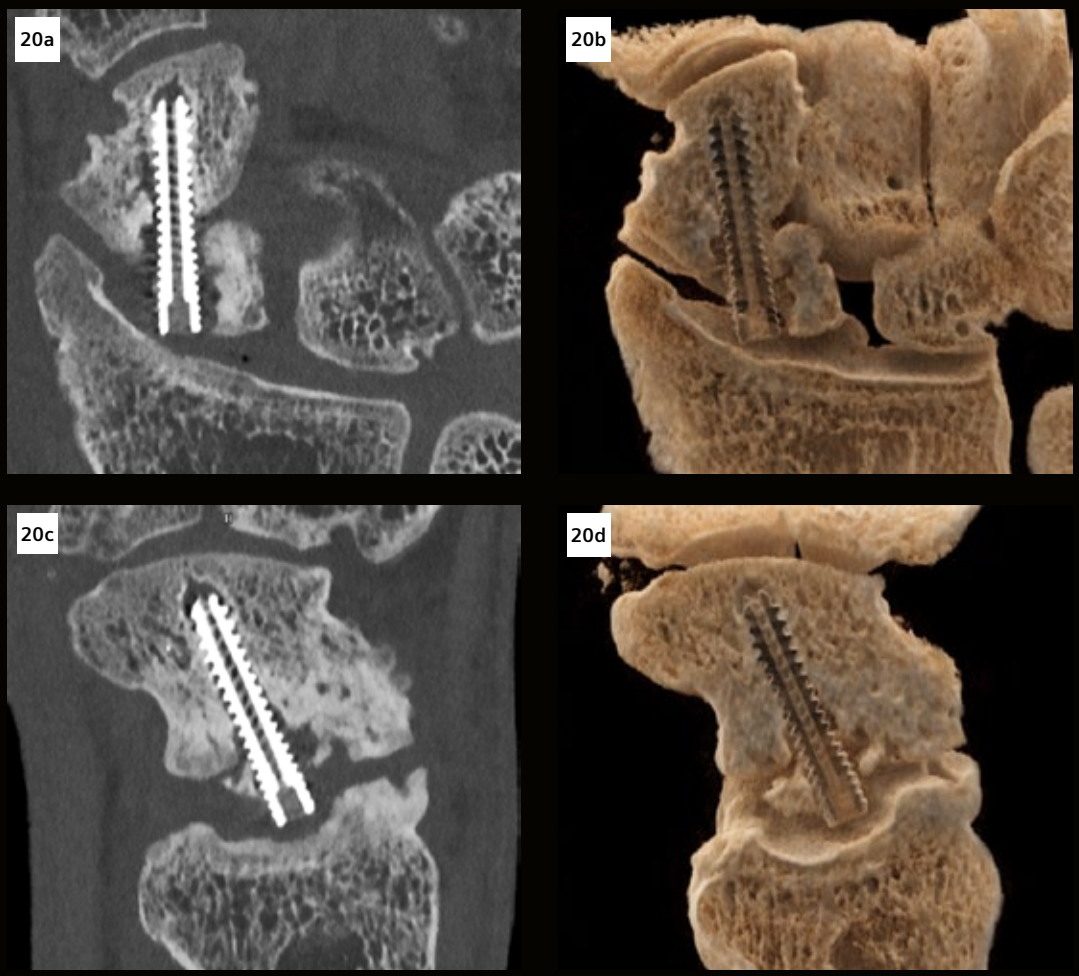

Figure 20: MPR images (Fig. 1a & 1c) and cVRT images (Fig. 1b & 1d), reconstructed parallel to the screw, show lucency on the tip of the screw and in various parts around the screw, confirming screw loosening. Metal artifact reduction surrounding the screw is remarkable, and the trabecular bone structure surrounding the fracture can be appreciated. The fracture in the scaphoid is still largely visible, with a sclerotically bordered fracture line. *Courtesy of Department of Radiology & Nuclear Medicine, Erasmus MC Rotterdam, Rotterdam, The Netherlands*

Pediatric imaging

Traditionally, the application of UHR in pediatric imaging has been problematic due to the high dose penalty associated with conventional EID-CT scanners. The advancement of Quantum HD technology has mitigated this dose penalty issue, making UHR imaging more feasible and beneficial for pediatric exams. For example, it has been demonstrated that reduced dose Quantum HD permits diagnostic CT image quality at radiation doses similar to that of chest radiography, while allowing reproducible cystic fibrosis grading (Brody II findings) [21]. This underscores the clinical value of UHR in pediatric imaging, particularly for conditions where frequent imaging is required [7], [21], [22], [23].

Additionally, increased resolution may translate to earlier detection of lung nodules, which is crucial for pediatric patients with cancer [22]. Specifically, enhanced resolution impacts decisions to perform metastasectomy, potentially improving outcomes for children with metastatic disease. Finally, a multi-center review paper provided a list of sample pediatric protocols over 50% of which include a UHR series (see Table 2), highlighting its growing importance and adoption in clinical practice [23].

	Dose4D & CARE keV	CARE keV optimized for	CARE kev IQ level	Effective mAs	kV	Pitch	Rotation time (s)	Scan Mode* (short name)	Collimation (mm)	Kernel
Chest without contrast	Manual	Non-contrast	35–45	Varies	120	3.2	0.25	Flash+SR+ME or Flash+UHR	144 × 0.4 (SR) or 120 × 0.2 (UHR)	Br44, Qr56
Chest with contrast	Manual	Soft Tissue	35–45	Varies	120	3.2	0.25	Flash+SR+ME	144 × 0.4	Br44, Qr56
Chest without contrast (low dose)	Manual	Non-contrast	2–6	Varies	Sn 100	3.2	0.25	Flash_UHR+Sn	120 × 0.2	Br44, Qr56
Abdomen Pelvis with contrast	Manual	Soft Tissue	120–140	Varies	120	3.2	0.25	Flash+SR+ME	144 × 0.4	Br44, Qr44
Abdomen Pelvis without contrast	Manual	Non-contrast	120–140	Varies	120	3.2	0.25	Flash+SR+ME	144 × 0.4	Br44
Extremity without contrast	Off	Off	Off	65-160	120	1	0.5-1	UHR+ME	120 × 0.2	Br76 to Br84
Extremity CTA	Manual	Vascular	120–140	Varies	120	0.5	0.25-1	UHR+ME	120 × 0.2	Bv38 to Bv60
Temporal Bone without contrast	Manual	Non-contrast	220	Varies	120	0.5	1	UHR+ME	120 × 0.2	Hr44, Hr84
Abdominal CTA	Manual	Vascular	120–180	Varies	120	0.5	0.25	UHR+ME	120 × 0.2	Bv38 to Bv60

Table 2: Sample pediatric protocols suggested by Horst et al. [23] heavily favor the inclusion of UHR series.

** SR = Standard Resolution; ME = Multienergy; UHR = Ultra High Resolution*

Case study

Pediatric cholesteatoma

Hunor Sükösd, MD; Éva Juhász, RT
Medical Imaging Centre, Semmelweis University, Budapest, Hungary

History

A 7-year-old girl presented with bilateral progressive conductive hearing loss, more pronounced on the left side. To assess the middle ear structures, a CT scan was indicated and performed using the Quantum HD mode on NAEOTOM Alpha.

Diagnosis

These images revealed a soft tissue mass in the left middle ear extending into the mastoid antrum. There was erosion of the long process of the incus and the stapes, with the eardrum and scutum intact, and Prussak's space was free. The findings were consistent with congenital cholesteatoma, Potsic stage IV. Surgical findings confirmed the CT diagnosis, and the patient was treated on the left side.

Conclusion

Congenital cholesteatomas, consisting of keratin debris and cholesterol, are common causes of pediatric conductive hearing loss. Early diagnosis is crucial to prevent extensive surgery and preserve hearing, especially since many children are asymptomatic and resist thorough examinations.

An optimized 70 kV protocol achieved a very low dose-length product (DLP) of only 92.3 mGy*cm, more than half of the typical DLPs of 200–400 mGy*cm for similar examinations. This is particularly beneficial for pediatric patients, who are more sensitive to radiation. See Figure 21.

Examination protocol	
Scan area	Temporal Bone
Scan mode	UHR mode
Scan length	53.8 mm
Scan direction	Caudo-cranial
Scan time	1.3 s
Tube voltage	70 kV
Effective mAs	340 mAs
Dose modulation	CARE Dose4D
$CTDI_{vol}$	13 mGy (16 cm phantom)
DLP	92.3 mGy*cm
Rotation time	0.5 s
Pitch	0.85
Slice collimation	120 × 0.2 mm
Slice width	0.2 mm
Reconstruction increment	0.2 mm
Reconstruction kernel	Hr84, QIR 3

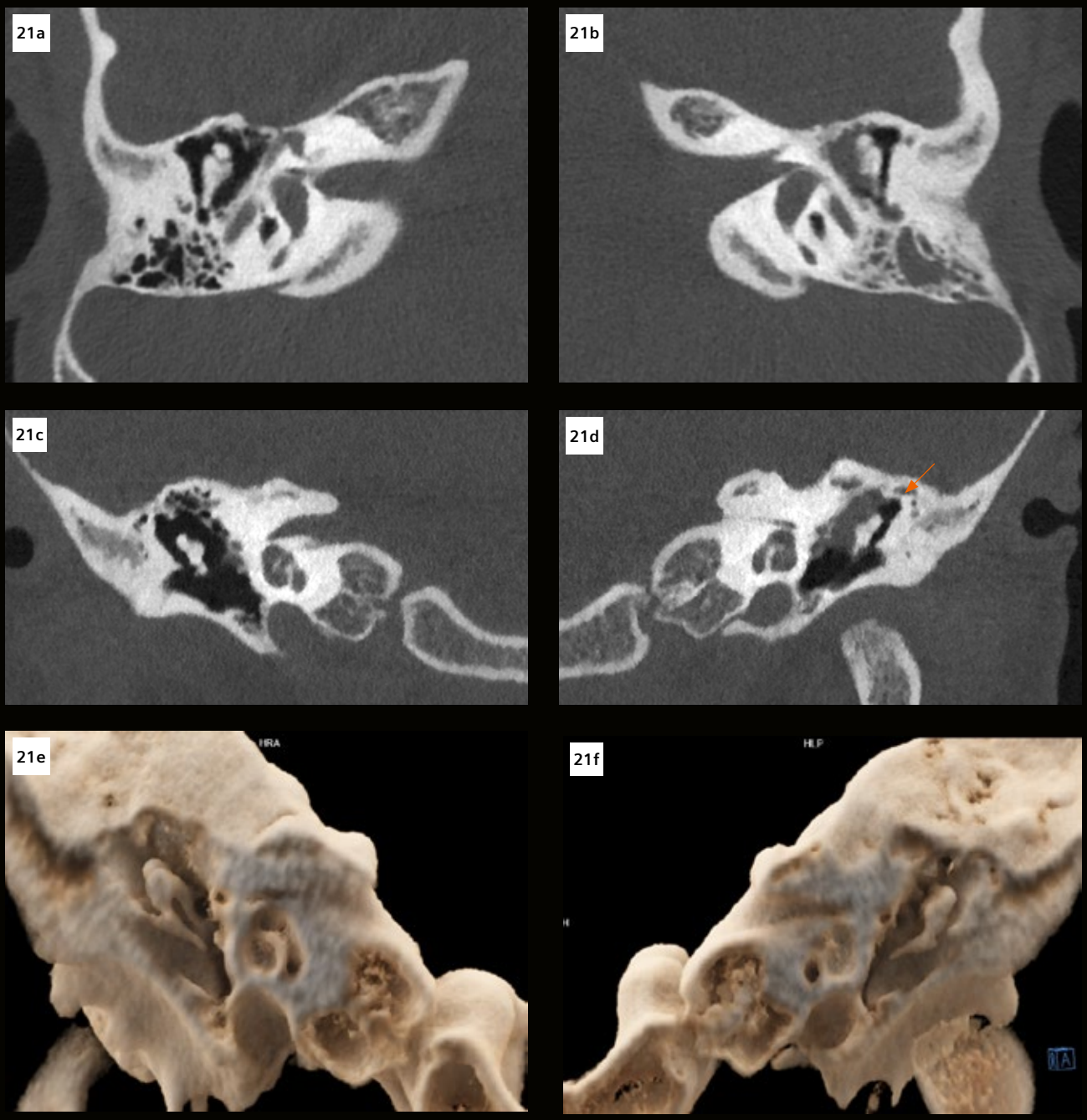

Figure 21: Axial images (Figs. 22a & 22b) and coronal MPR images (Figs. 22c & 22d) show a soft tissue mass in the left middle ear, eroding the long process of the incus and the stapes. The Prussak's space (Fig. 22d, arrow) is free and the scutum was intact. No remarkable findings on the right side. cVRT images (Figs. 22e & 22f) show a 3D view of bilateral ossicles – normal on the right and eroded on the left. Note that the input images for cVRT creation are the UHR images reconstructed at 0.2 mm with a very sharp kernel of Hr84. *Courtesy of Medical Imaging Centre, Semmelweis University, Budapest, Hungary.*

Cardiovascular imaging

On NAEOTOM Alpha, in the cardiovascular domain, UHR is known as Quantum HD Cardiac. With typical size of coronary vessels of around 1 to 4 mm, Quantum HD Cardiac may benefit the accurate assessment of such small vasculature. Additionally, it may facilitate observing even smaller plaques and calcifications or evaluating stent patency not previously possible. Since calcium blooming is related to the partial volume effect, enabling high resolution reconstruction capabilities is an alternative non-spectral approach to solve this critical clinical challenge.

Coronary stenosis

In evaluating coronary stenosis, many studies [24]–[27] have reported a downgrading or reclassification of Coronary Artery Disease Reporting and Data System (CAD-RADS) scores due to Quantum HD Cardiac's ability to provide "sharper images of coronary arteries, a superior coronary plaque delineation, a reduction of partial volume effects, and fewer blooming artifacts," [26] compared to conventional EID-CT. Specifically, it has been demonstrated that Quantum HD Cardiac "allowed for a reclassification of 54% of patients toward a lower Coronary Artery Disease Reporting and Data System category compared with standard spatial

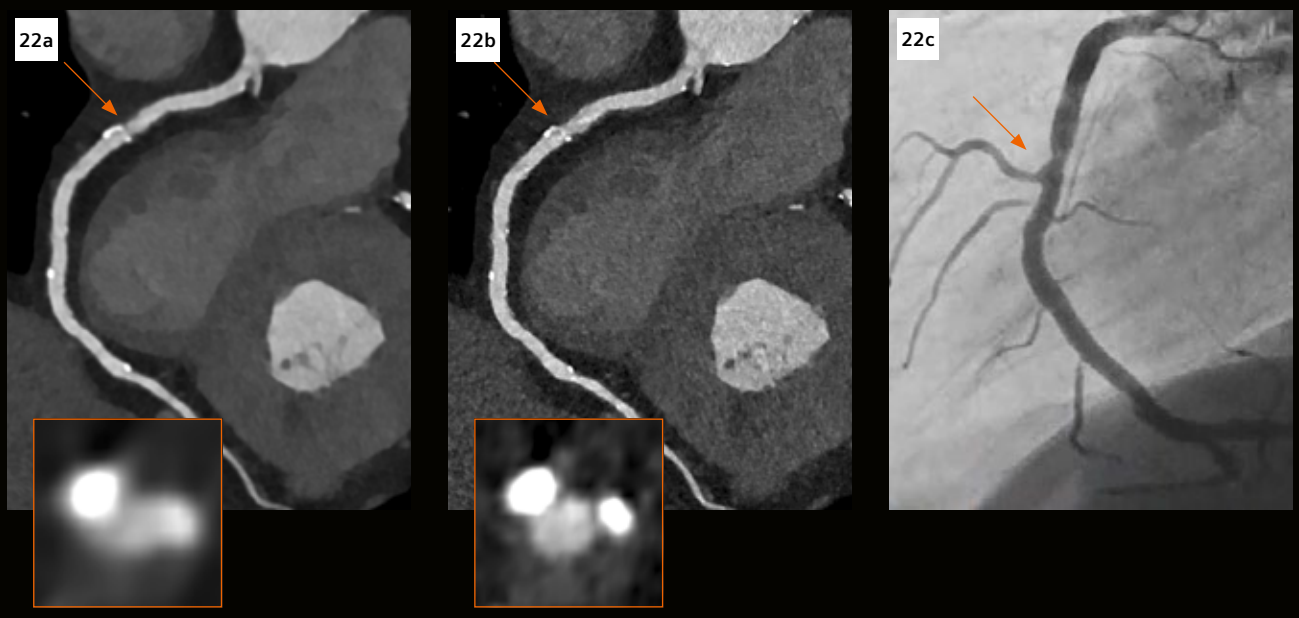

Figure 22: Curved MPR images (Figs. 22a & 22b) show a proximal RCA stenosis caused by calcified plaques (arrows). Images are reconstructed at 0.6 mm with kernel Bv40 (Fig. 22a) and at 0.2 mm with kernel Bv60 (Fig. 22b). The corresponding axial slices, perpendicular to the vessel centerlines at the stenosis, are shown in the left lower corners. The blooming effect of the calcified plaques affecting the visualization of the vessel lumen and the stenosis grading is clearly reduced in the UHR images. An invasive catheter coronary angiography (Fig. 22c) confirmed a mild stenosis in the proximal RCA (arrow) consistent with the result from the UHR image evaluation.
Courtey of University Hospital Zurich, Zurich, Switzerland.

resolution," [27]. This regrading of CAD-RADS for patients undergoing coronary evaluation can also be seen in Figure 22, where Quantum HD Cardiac provided a downgrading of CAD-RADS from grade 3 to grade 2, which "altered the care plan" for this [28]. On a larger scale, an 812-patient study reported that "in patients who underwent CCTA with PCCT the number of subsequent ICAs (Invasive Coronary Angiography) was lower as compared to patients who were scanned with EID-CT. This difference was greater in patients with extensive coronary calcification," which suggests that "PCCT improves clinical efficacy, as the number of invasive examinations could be decreased" [28].

Stent patency

Quantum HD Cardiac can also play a role in evaluating stent patency. The presence of heavy calcifications in a stented segment may exacerbate any artifacts due to the stent material itself. The small pixel sizes associated with Quantum HD Cardiac, however, may reduce the partial volume effects and therefore calcium blooming (Figure 23). In one study evaluating coronary artery segments, it was shown that out of 1080 evaluated coronary segments in 60 patients, 85% had "excellent or very good image quality", suggesting that "UHR PCCT can play an essential role in the evaluation of coronary stents and in-stent restenosis" [29] (see Figure 23).

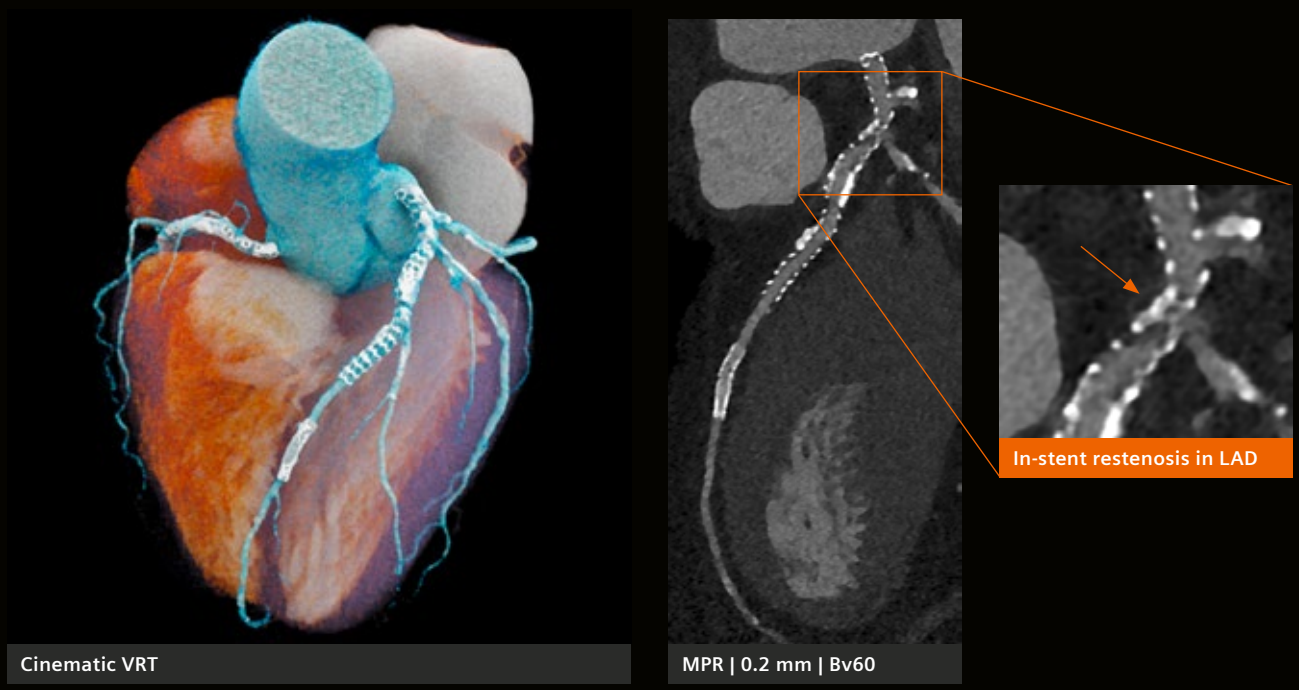

Figure 23: Stent imaged in Quantum HD Cardiac mode (Bv72, 1024 × 1024, QIR 4, 0.2 mm slice thickness) on NAEOTOM Alpha, demonstrating in-stent restenosis. The patient underwent coronary stent implantation multiple times and had 8 stents implanted in total in the left and right coronary arteries. The orange arrow shows a focal, severe in-stent restenosis at the ostium of the LAD. MPR 0.2 mm (Fig23a) | Cinematic VRT (Fig 23b) | Bv56 | 140 kV | $CTDI_{vol}$ 22.5 mGy.
Courtesy of Semmelweiss University Hospital, Budapest, Hungary.

Plaque Quantification

Due to calcium blooming, it can be difficult to accurately assess calcified lesions. A high coronary calcium burden may lead to an overestimation of the degree of stenosis and a false-positive diagnosis. In such cases, Quantum HD Cardiac, employing a sharp vascular kernel, may improve the visualization of these highly calcified plaques (Figure 24). In this high-risk population, "UHR photon-counting CCTA provided high diagnostic accuracy in the detection of CAD ... including subjects with severe coronary calcification" [30].

The Future: New Quantum HD Cardiac features and AI-tools

Motion artifacts from patient breathing or movement can adversely influence cardiac assessment and diagnosis. This can manifest as discontinuities along the range of acquisition (e.g., for sequential ECG-gated scanning this may appear as a stair step at the image stack transition). ZeeFree, a new reconstruction-stage algorithm, can mitigate the appearance of these misalignments. Quantum HD may be paired with ZeeFree.

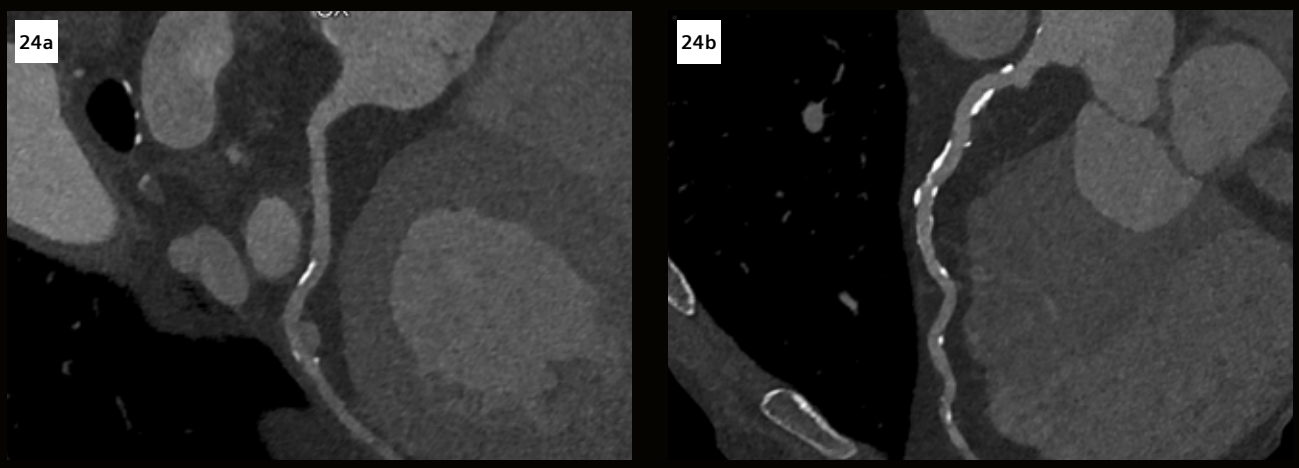

Figure 24: Coronary CTA using Quantum HD Cardiac in patient with calcium score of 1758. Curved MPR 0.2 mm (Fig 24a–c) | Cinematic VRT (Fig. 24d) | Bv56 | 120 kV | $CTDI_{vol}$ 19.6 mGy.
Courtesy of Semmelweis University, Budapest, Hungary

Another recent technological advancement in Quantum HD Cardiac is the optional inclusion of spectral information. This allows for the reconstruction of both UHR and spectral image volumes from a single acquisition. Stent evaluation may benefit from this feature.

"At our institution we expect to send fewer patients to the cath lab for diagnostic imaging and do a photon-counting CT instead."

Richard Bayer, MD · Cardiologist MUSC, Charleston, SC, USA

Finally, tools for semi-automatic and automatic coronary vessel and plaque assessment are firmly established in the cardiac imaging community. However, these AI tools have been trained and evaluated on conventional EID-CT data. It will be exciting to see what effect the introduction of Quantum HD Cardiac will have on this technology.

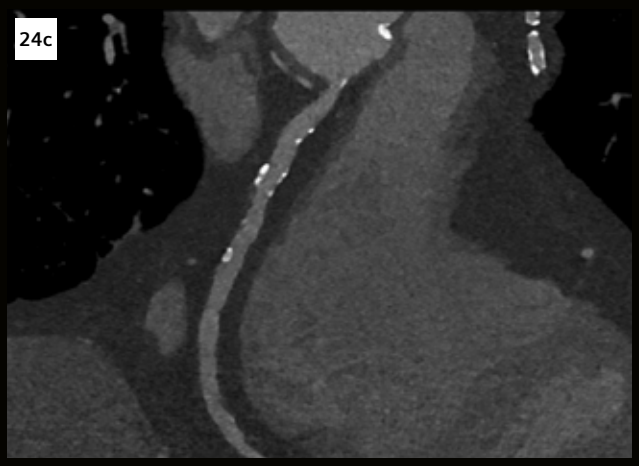

24c

24d

Case study

Extensive coronary calcifications with high-risk plaques

Muhammad Taha Hagar, MD; Prof. Christopher L. Schlett, MD, MPH; Prof. Fabian Bamberg, MD
Department of Diagnostic and Interventional Radiology, University Medical Center Freiburg, Germany

History

A 64-year-old male patient presented himself to the hospital complaining of atypical chest discomfort during exercise and palpitations at rest. In a recent stress-ECG examination, ventricular extrasystoles were observed during the maximum exercise phase and the primary post-exercise phase. Given the low to intermediate pretest probability of coronary artery disease (CAD), in line with current international guidelines [31], a CCTA was performed using Quantum HD Cardiac to rule out exercise-induced coronary insufficiency as a potential underlying cause of his symptoms.

Diagnosis

Quantum HD Cardiac mode was selected for CCTA which provided diagnostic images – two mixed plaques with high-risk features in the proximal LAD and RCA were evident, characterized by a hypoattenuating plaque component (< 30 HU) and positive remodeling. Mild coronary stenoses (25–49%) were visualized in the proximal LAD and RCA. The circumflex (Cx) showed non-calcified plaques, however, it was free from stenosis. The left ventricle was of a normal size, with a normal ejection fraction (EF) of 69%, without any hypertrophy. According to the CAD-RADS 2.0 consensus statements [25], this patient's CCTA was classified as CAD-RADS 2/P4/HRP. Subsequently, the patient was referred to an outpatient cardiologist. Risk factor modification, intensive preventive pharmacotherapy with statins, and a short-term clinical follow-up were recommended.

Examination protocol	
Scan area	Heart
Scan mode	CCTA, UHR mode
Scan length	124.5 mm
Scan direction	Cranio-caudal
Scan time	8.8 s
Tube voltage	120 kV
Effective mAs	48 mAs
Dose modulation	CARE Dose4D
CTDIvol	29.9 mGy
DLP	421 mGy*cm
Rotation time	0.25 s
Pitch	0.15
Slice collimation	120 × 0.2 mm
Slice width	0.2 mm
Reconstruction increment	0.1 mm
Reconstruction kernel	Bv64, QIR 4
Reconstruction matrix	1024 × 1024
Heart rate	51 bpm
Contrast	370 mg/mL
Volume	85 mL + 49 mL saline
Flow rate	6 mL/s
Start delay	Test Bolus

Comments

Identifying the high risk plaque (HRP) features in CT imaging requires optimal spatial and temporal resolution, as well as minimization of blooming interference caused by calcified plaques. This case employed Quantum HD Cardiac mode with a sharp kernel (Bv64) for image reconstruction, only available on NAEOTOM Alpha [32]. Recent clinical studies have reported an impressive success rate and diagnostic accuracy using this mode for coronary evaluation, even in the presence of extensive calcification [30].

As shown in this case, CCTA with Quantum HD Cardiac provides crucial information about the patient's cardiac health even in the presence of severe coronary calcifications – it helps the physicians identify HRP and rule out obstructive coronary artery disease. Owing to the optimal image quality achieved by Quantum HD Cardiac, CT findings help in patient risk stratification and guiding patient management. As this patient did not need to undergo invasive angiography after CT evaluation, the associated cost could be reduced.

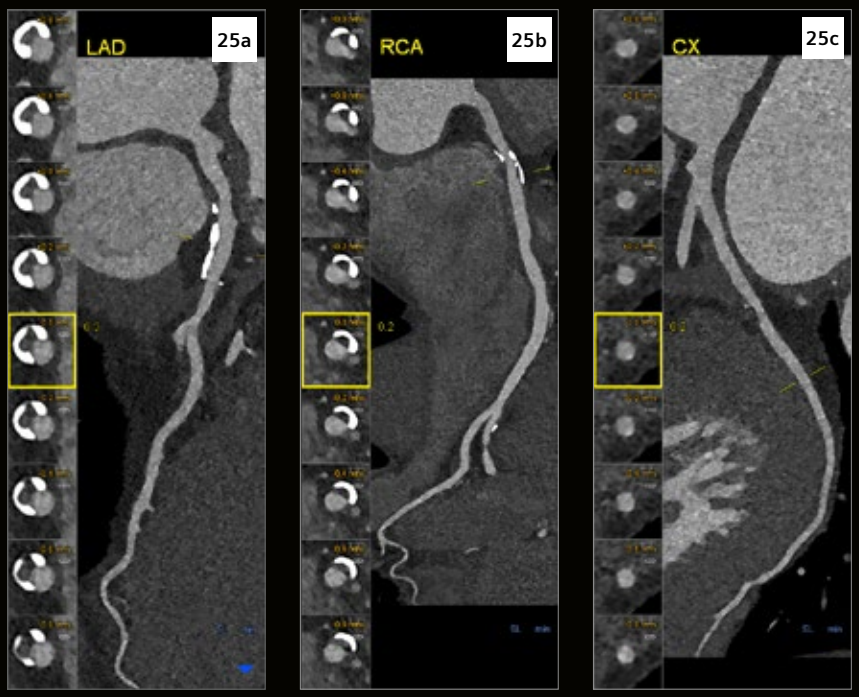

Figure 25: Curved MPR (0.2 mm) of the coronary arteries reveal non-obstructive stenoses (< 50%) in the proximal LAD (Fig. 25a) and RCA (Fig. 25b) with a clear lumen exhibiting no noticeable blooming artifact interference despite the presence of extensive calcifications. Two mixed plaques with high-risk features, characterized by a hypoattenuating plaque component (< 30 HU) and positive remodeling, are evident in the proximal LAD and RCA. The Cx (Fig. 25c) shows non-calcified plaques, and is free from stenosis.
Courtesy of Department of Diagnostic and Interventional Radiology, University Medical Center Freiburg, Freiburg, Germany.

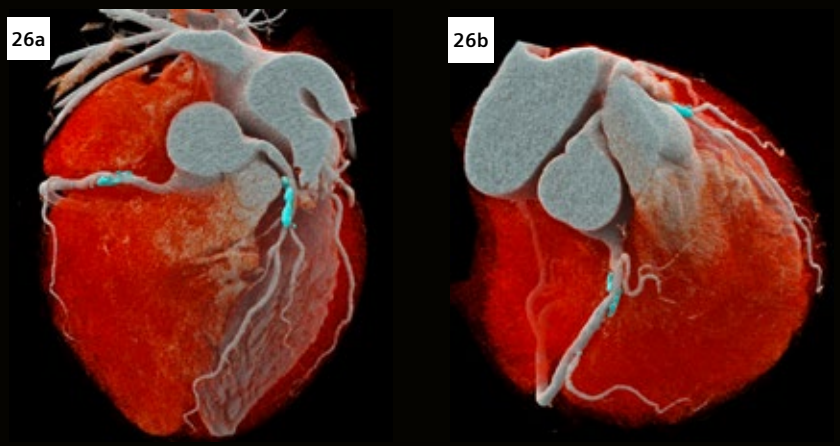

Figure 26: Three-dimensional Cinematic VRT images highlight the calcified plaques in the proximal LAD and RCA (in blue). Note that the images used for the rendering are reconstructed at 0.2 mm with a sharp kernel of Bv64.
Courtesy of Department of Diagnostic and Interventional Radiology, University Medical Center Freiburg, Freiburg, Germany.

Conclusion

Quantum HD technology represents a transformative step in medical imaging. It can detect and visualize minute anatomical details with a high level of clarity, potentially facilitating early diagnosis, at low radiation doses.

The cases reviewed here, from pediatric imaging to the detection of cerebrospinal fluid venous fistulas and thoracic abnormalities, underscore the value of Quantum HD in the clinic. In the neurological domain, its ability to enhance the visibility of delicate structures and subtle pathologies stands out, improving diagnostic confidence. Similarly, in musculoskeletal imaging, it has been demonstrated that the sharp delineation of bone structures can impact the assessment of fractures and surgical planning.

As the field advances, the integration of Quantum HD with spectral imaging has the potential for even greater diagnostic capabilities.

Ultimately, Quantum HD imaging is not just a technological upgrade but a paradigm shift that enhances the precision, efficiency, and impact of medical imaging. Its growing adoption across various clinical specialties heralds a new era of diagnostic confidence, supporting the clinician in spotting the small details - often the most critical. The journey toward even higher standards of care continues, driven by the pursuit of innovation and excellence in imaging technology.


SIEMENS
Healthineers
NAEOTOM Alpha

References

[1] Gaillandre Y, Duhamel A, Flohr T, Faivre JB, Khung S, Hutt A, et al. (2023). Ultra-high resolution CT imaging of interstitial lung disease: impact of photon-counting CT in 112 patients. European Radiology, 33(8), 5528–5539.

[2] Inoue A, Johnson TF, White D, Cox CW, Hartman TE, Thorne JE, et al. (2022). Estimating the clinical impact of photon-counting-detector CT in diagnosing usual interstitial pneumonia. Investigative Radiology, 57(11), 734–741.

[3] Prayer F, Kienast P, Strassl A, Moser PT, Bernitzky D, Milacek C, et al. (2023). Detection of post-COVID-19 lung abnormalities: Photon-counting CT versus same-day energy-integrating detector CT. Radiology, 307(1). doi:10.1148/radiol.222921.

[4] Brandt EGS, Müller CF, Thomsen H, Rodell AB, Ibragimov B, Andersen MB. (2024). Imaging the pancreas with photon-counting CT – A review of normal pancreatic anatomy. European Journal of Radiology, 181, 111736.

[5] Díez M, Teulé A, Salazar R. (2013). Gastroenteropancreatic neuroendocrine tumors: diagnosis and treatment. Annals of Gastroenterology, 26(1), 29–36.

[6] Flohr T, et al. (2020). Photon-counting CT review. Physica Medica, 79, 126–136.

[7] Joshi VM, Navlekar SK, Kishore GR, et al. (2012). CT and MR imaging of the inner ear and brain in children with congenital sensorineural hearing loss. Radiographics, 32(3), 683–698.

[8] Hermans J, De Coninck T, Dymarkowski S, et al. (2023). Comparison of NAEOTOM Alpha and SOMATOM Force for ultra-high-resolution temporal bone imaging: image quality and diagnostic performance. Insights into Imaging, 14(1), 180. doi:10.1186/s13244-023-01472-y.

[9] Farnsworth TJ, Schwartz M, Lerman A, et al. (2023). Ultra-high-resolution photon-counting CT angiography of the orbits: comparison with dual-source CT. Interventional Neuroradiology. doi:10.1177/15910199231189054.

[10] Madhavan R, Schwartz M, Lee M, et al. (2024). Photon-counting CT in neurovascular imaging: clinical applications and performance characteristics. The British Journal of Radiology, 97(1156), 20230721. doi:10.1259/bjr.20230721.

[11] Schwartz M, Madhavan R, Lee M, et al. (2024). Comparison of photon-counting detector CT and energy-integrating detector CT in spinal CSF venous fistula detection using CT myelography. American Journal of Roentgenology, 222(2), 290–297. doi:10.2214/AJR.23.29913.

[12] Madhavan R, Schwartz M, Lee M, et al. (2023). Photon-counting CT myelography improves detection of spinal CSF venous fistulas in the lateral decubitus position: diagnostic performance and implications for clinical workflow. American Journal of Neuroradiology, 44(7), 828–834. doi:10.3174/ajnr.A8078.

[13] Madhavan R, Schwartz M, Lee M, et al. (2023). Decubitus positioning improves CT myelographic detection of spinal CSF venous fistulas: diagnostic performance of photon-counting detector CT. American Journal of Neuroradiology, 44(11), 1583–1589. doi:10.3174/ajnr.A8033.

[14] Booij R, van der Meijden D, van Stralen M, et al. (2022). Ultra-high-resolution imaging of the wrist with photon-counting CT at half the radiation dose: a cadaver study. European Journal of Radiology, 157, 110694. doi:10.1016/j.ejrad.2022.110694.

[15] Sonnow L, May M, Lell MM, et al. (2023). Ultra-high-resolution imaging of elbow joint fractures: a cadaver study using photon-counting detector CT. European Radiology Experimental, 7(1), 25. doi:10.1186/s41747-023-00346-4.

[16] Kammerling N, Booij R, Müller FC, et al. (2024). Diagnosing and following up scaphoid fractures using 140Sn ultra-high-resolution photon-counting CT versus dual-source CT: a comparative study. European Journal of Radiology, 168, 111304. doi:10.1016/j.ejrad.2024.111304.

[17] Thomsen H, Brandt EGS, Ahlström H, et al. (2022). Photon-counting CT of the wrist: Can it visualize trabecular structures? Comparison with HR-pQCT. Investigative Radiology, 57(7), 443–451. doi:10.1097/RLI.0000000000000874.

[18] Bette S, Beer L, Tsagkrasoulis D, et al. (2024). Photon-counting detector CT in musculoskeletal radiology: Initial clinical experience and diagnostic performance. RoFo – Fortschritte auf dem Gebiet der Röntgenstrahlen und der bildgebenden Verfahren. doi:10.1055/a-2183-1851.

[19] van Bergen CJ, van den Ende KI, Ten Brinke B, Eygendaal D. (2016). Osteochondritis dissecans of the capitellum in adolescents. World Journal of Orthopedics, 7(2), 102–108. doi:10.5312/wjo.v7.i2.102.

[20] van den Ende KIM, Keijsers R, van den Bekerom MPJ, Eygendaal D. (2019). Imaging and classification of osteochondritis dissecans of the capitellum: X-ray, magnetic resonance imaging or computed tomography? Shoulder & Elbow, 11(2), 129–136. doi:10.1177/1758573218756866.

[21] Horst KK, Hull NC, Thacker PG, et al. (2023). Reduced-dose photon-counting detector CT for Brody II scoring in children with cystic fibrosis: a pilot study. Pediatric Radiology, 53(6), 1049–1056. doi:10.1007/s00247-022-05574-6.

[22] Cao L, Schwartz M, Madhavan R, et al. (2022). Pediatric applications of photon-counting CT: initial clinical experience. American Journal of Roentgenology, 219(6), 971–978. doi:10.2214/AJR.22.28066.

[23] Horst KK, Hull NC, Demirel N, et al. (2023). Photon-counting CT in pediatric imaging: review of potential benefits and early experience. British Journal of Radiology, 96(1149), 20230221. doi:10.1259/bjr.20230221.

[24] Koons PN, Rajendran K, Horst KK, et al. (2023). Coronary stenosis quantification in patients with dense calcifications using ultra-high-resolution photon-counting CT vs dual-source CT. Journal of Cardiovascular Computed Tomography, 17(6), 689–695. doi:10.1016/j.jcct.2023.10.003.

[25] McCollough CH, Carter RE, Rajendran K, et al. (2024). Visual estimation of coronary artery stenosis severity: Photon-counting CT versus dual-source CT. Radiology, 310(2), e230168. doi:10.1148/radiol.230168.

[26] Eberhard M, Taron J, Maintz D, et al. (2023). Coronary stenosis quantification using ultra-high-resolution photon-counting CT versus invasive coronary angiography. JACC: Cardiovascular Imaging. doi:10.1016/j.jcmg.2023.10.011.

[27] Halfmann MC, Maintz D, Chicaiza DF, et al. (2024). Ultra-high-resolution coronary CT angiography with photon-counting detector CT for coronary stenosis assessment. Radiology, 310(3), e231030. doi:10.1148/radiol.231030.

[28] Simon A, Müller C, Bratke G, et al. (2023). Rate of invasive coronary angiography recommendations after coronary CT angiography: Comparison of photon-counting CT and CardioGraphe. Journal of Cardiovascular Computed Tomography. doi:10.1016/j.jcct.2023.12.007.

[29] van der Bie SC, Booij R, de Graaf MA, et al. (2024). Coronary segment image quality assessment using photon-counting CT: comparison with dual-source CT. European Journal of Radiology, 169, 111471. doi:10.1016/j.ejrad.2024.111471.

[30] Hagar MT, Rajendran K, Madhavan R, et al. (2023). Accuracy of ultrahigh-resolution photon-counting CT for detecting coronary artery disease in a high-risk population. Radiology, 307, e223305. doi:10.1148/radiol.223305.

[31] Knuuti J, Wijns W, Saraste A, et al. (2020). 2019 ESC guidelines for the diagnosis and management of chronic coronary syndromes. Russian Journal of Cardiology, 25, 119–180. doi:10.15829/1560-4071-2020-2-3757.

[32] Mergen V, van der Werf NR, Maintz D, et al. (2022). Ultra-high-resolution coronary CT angiography with photon-counting detector CT: feasibility and image characterization. Investigative Radiology. doi:10.1097/RLI.0000000000000897.

At Siemens Healthineers, we pioneer breakthroughs in healthcare. For everyone. Everywhere. Sustainably. As a market leader, we want to advance a world in which breakthroughs in healthcare create new possibilities with a minimal impact on our planet. We've been pushing the boundaries in medical technology for more than 125 years. By consistently bringing innovations to the market, we enable healthcare professionals to innovate personalized care, achieve operational excellence, and transform the system of care.

With the unique combination of our strengths in patient twinning[1], precision therapy, as well as digital, data, and artificial intelligence (AI), we are well positioned to take on the greatest challenges in healthcare. We will continue to build on these strengths to help overcome the world's most threatening diseases, enable efficient operations, and expand access to care.

Our portfolio, spanning in-vitro and in-vivo diagnostics to image-guided therapy and cancer care, is crucial for clinical decision-making and treatment pathways. We are committed to improving healthcare access for all, limiting our environmental impact as we pioneer breakthroughs, and engaging our diverse Healthineers to achieve this impact on a global scale.

Motivated by our purpose and guided by our values, we are building an inclusive culture, where we embrace diversity in all its forms. We are a team of 73,000 Healthineers in over 70 countries passionately pushing the boundaries of what is possible in healthcare to help improve the lives of people around the world.

[1] *Personalization of diagnosis, therapy selection, and monitoring, aftercare, and managing health.*

The statements by customers of Siemens Healthineers described herein are based on results that were achieved in the customer's unique setting. Because there is no "typical" hospital and many variables exist (e.g., hospital size, case mix, level of IT and/or automation adoption) there can be no guarantee that other customers will achieve the same results.

The products/features (mentioned herein) are not commercially available in all countries. Their future availability cannot be guaranteed.

On account of certain regional limitations of sales rights and service availability, we cannot guarantee that all products included in this brochure are available through the Siemens Healthineers sales organization worldwide.

Availability and packaging may vary by country and are subject to change without prior notice. Some/All of the features and products described herein may not be available in the United States.

The information in this document contains general technical descriptions of specifications and options as well as standard and optional features that do not always have to be present in individual cases.

Siemens Healthineers reserves the right to modify the design, packaging, specifications, and options described herein without prior notice. Please contact your local Siemens Healthineers sales representative for the most current information.

Note: Any technical data contained in this document may vary within defined tolerances. Original images always lose a certain amount of detail when reproduced.

Siemens Healthineers Headquarters
Siemens Healthineers AG
Siemensstr. 3
91301 Forchheim, Germany
Phone: +49 9191 18-0
siemens-healthineers.com

Published by Siemens Healthineers AG · Order No. CT-00112-16C1-7600 · Printed in Germany · 15677 0825 · *©Siemens Healthineers AG, 2025*